A model for simulation of the climate and hydrology of the Great Lakes basin

Brent M. Lofgren

Great Lakes Environmental Research Laboratory, NOAA, Ann Arbor, Michigan, USA

Received 4 February 2004; revised 13 May 2004; accepted 24 June 2004; published 23 September 2004.

[1] The Coupled Hydrosphere-Atmosphere Research Model (CHARM) was developed by coupling the Regional Atmospheric Modeling System (RAMS) to models of the land hydrology of the Great Lakes basin and of the evaporation and thermodynamics of the Great Lakes. It is intended for running coupled atmosphere-surface climate scenarios for the Great Lakes basin, to gain a perspective that has been missed by running hydrologic models in off-line mode, driven by the output of global general circulation models. This paper presents validation of this model using historical atmospheric data to drive the regional embedded CHARM model. The current version of CHARM simulates the near-surface air temperature in the region quite well, with some positive bias during the winter and negative bias during the summer. Biases in the temperature averaged over 1 month and over the portion of the domain that is not directly forced by observations are less than or approximately 2 K. The annual precipitation has a positive bias of 6.6% and does well at placing the lake-effect precipitation areas, but may have too strong a west-east gradient. Simulation of annually averaged runoff meets well with expectations, but additional empirical fitting may be required to replicate the seasonal cycle. Aspects of the model that remain troublesome are the tendency for unrealistically low pressure at mean sea level and for persistent heavy low stratus clouds. *INDEX TERMS:* 1620 Global Change: Climate dynamics (3309); 1655 Global Change: Water cycles (1836); 1833 Hydrology: Hydroclimatology; 3337 Meteorology and Atmospheric Dynamics: Numerical modeling and data assimilation; *KEYWORDS:* atmospheric/lake interactions, regional climate modeling, hydroclimatology

Citation: Lofgren, B. M. (2004), A model for simulation of the climate and hydrology of the Great Lakes basin, *J. Geophys. Res.*, *109*, D18108, doi:10.1029/2004JD004602.

1. Introduction

[2] Climate change and its effects on water resources are of concern in many regions, including the North American Great Lakes basin. The water depth within channels, harbors, and marinas can have a great effect on the economic sectors of commercial shipping and recreational boating. The concerns of shoreline residents and for the maintenance of healthy shoreline wetland ecosystems can be affected by fluctuations and trends in lake level. One factor that makes the net supply of water (precipitation minus evaporation) to the Great Lakes basin sensitive to changes in climate is that 33% of the basin's area is covered by the Great Lakes themselves [*Coordinating Committee on Great Lakes Basic Hydraulic and Hydrologic Data*, 1977]. Over water bodies, evaporation is not regulated by the availability of water as it is on land, but by available energy, so changes in the energy budget of the surface result more directly in changes in the outflow from the lakes into their connecting channels and their eventual drain through the St. Lawrence River.

[3] The Laurentian Great Lakes help to shape their own meteorological and hydrological environment. Lakes Erie, Huron, Michigan, Ontario, St. Clair, and Superior collectively cover a total surface area of approximately 245,000 km^2 and have a water volume of approximately 22,700 km^3. The high thermal inertia of these water bodies causes their interface with the atmosphere to contrast sharply with the surrounding land as well as the other, shallower lakes scattered around the region. Their remoteness from the oceans further highlights these influences. Lake-effect snow [e.g., *Hjelmfelt and Braham*, 1983; *Hjelmfelt*, 1990], lake breeze [e.g., *Lyons and Cole*, 1976], and midlake cloud bands [*Hjelmfelt and Braham*, 1983] are well-known short-term phenomena that occur on the scale of individual lakes. *Sousounis and Shirer* [1992] and *Sousounis and Fritsch* [1994] have highlighted "lake-aggregate" thermal effects that are capable of causing the weakening, strengthening, or splitting of surface synoptic-scale meteorological systems.

[4] Concurrent with these relatively short-term meteorological phenomena that stem from the Great Lakes' influence on the atmosphere are global-scale changes in climate forcing due to increasing concentration of greenhouse gases [e.g., *Stouffer and Manabe*, 1999; *Manabe and Stouffer*, 1994; *Boer et al.*, 2000; *Gordon et al.*, 2000; *Hansen et al.*, 1988; *Intergovernmental Panel on Climate Change*, 1990, 1996, 2001]. Also, there are more localized, although

often long-term, effects on the storage, evaporation, and runoff of water influencing the Great Lakes system. Studies have been carried out at the Great Lakes Environmental Research Laboratory (GLERL) using the output of general circulation model (GCM) greenhouse warming scenarios as forcing for models of the Great Lakes thermodynamics and the hydrology of surrounding land surfaces [*Croley and Hartmann*, 1989; *Croley*, 1990; *Hartmann*, 1990; *Croley et al.*, 1991; *Lofgren et al.*, 2002; *Croley*, 2003]. These have used various approaches to the difficult issue of downscaling the coarse-gridded output of GCMs to the size of drainage basins of interest, but none have included two-way interaction in which the lakes are not only affected by the atmosphere, but the atmosphere is also affected by the lakes.

[5] The Great Lakes region's climatic response to increased greenhouse gases is dependent not only on externally forced changes in radiative forcing and the characteristics of air advected into the region, but also on the locally induced effects on daily weather, which in turn are dependent on the thermodynamic and evaporative characteristics of the region's lake and land surfaces. Additionally, lake surface temperature, soil moisture, runoff, and other hydrologic variables are dependent on the accompanying meteorological conditions. Therefore, although lake-effect snow, midlake cloud bands, lake breeze, and lake-aggregate thermal effects on synoptic cyclones can be demonstrated using atmospheric simulations of only a few days' duration and prescribed conditions of the surface (lake surface temperature, soil moisture, etc.), a more complete picture of surface-atmosphere interactions can be built on monthly to decadal timescales using a coupled model.

[6] The Coupled Hydrosphere-Atmosphere Research Model (CHARM) is intended to improve the simulation of climate and water resources in the Great Lakes region, in comparison to the global-scale climate models commonly used in the past. This is accomplished by putting a regional atmospheric model into direct contact with a model of lake thermodynamics, surface temperature, and heat transfer, especially designed for the Great Lakes, and a model of land processes, including evapotranspiration, surface runoff, soil moisture storage, snowmelt, percolation, interflow from soil and groundwater to surface storage, and outflow from surface storage. This regional approach enables enhanced spatial resolution compared to global models. Some of the benefits of this enhanced spatial resolution include the ability to explicitly simulate smaller-scale atmospheric phenomena and to resolve smaller features of the surface that affect the forcing of the atmosphere-water bodies most importantly in our case, but also topography and land use.

[7] This regional modeling approach has been taken by a number of other research groups. Examples include *Dickinson et al.* [1989], *Giorgi and Bates* [1989], and many more recent sources. Some previous studies [*Bates et al.*, 1993, 1995; *Hostetler et al.*, 1993] have concentrated on the Great Lakes in particular. However, CHARM differs from these in its emphasis on the simulation of the two-way interaction including the atmosphere's influence on surface, riverine, and lacustrine hydrology, rather than primarily looking at the atmosphere, with the surface as a boundary condition. In another study [*Goyette et al.*, 2000], a thermodynamic model of the Laurentian Great Lakes was developed for use within a regional climate model. This model used some large quantities of thermal flux correction to the lake temperatures, which certainly aid in producing valid lake surface temperatures, but can bias the lake-atmosphere heat fluxes, a major driver of the atmosphere.

[8] The CHARM project as a whole aims to develop a model coupling the atmosphere of the Great Lakes region to the land and lake surfaces, resulting in simulations of regional hydrology that are more plausible than those using off-line hydrologic models. This has the potential to be applied to decadal or longer scenarios of interest with regard to global warming and land-use change (such as conversion from forests to agricultural lands, from rural landscapes to impermeable urban landscapes, or from wetlands), or to shorter-term climatic effects due to remote influences by circulation patterns such as those associated with El Niño–Southern Oscillation.

[9] The present paper has a more limited scope; model formulation and validation of model variables will be presented. Unfortunately, close validation of many aspects of interaction between the atmosphere, the lakes, and the hydrologic system are not supported by the ready availability of instrumental data (e.g., air temperature and humidity gradients near shorelines, cloud cover contrasts between land and water areas). Therefore validation will be more general, mostly examining broad-scale atmospheric variable fields, and noting where apparent lake signatures occur, without a strong basis for evaluating the realism of their magnitude or exact location.

2. Model Formulation

[10] The CHARM is based on version 3a of the Regional Atmospheric Modeling System (RAMS), initially developed at Colorado State University, with further development by ASTER, Inc. [*Pielke et al.*, 1992] and current distribution of newer versions by ATMET. It is based on a combination of a nonhydrostatic cloud model described by *Tripoli and Cotton* [1982] and two hydrostatic mesoscale models [*Tremback et al.*, 1985; *Mahrer and Pielke*, 1977]. The development of CHARM is an effort to develop a regional climate model based on RAMS, independent from the work of *Liston and Pielke* [2001].

[11] RAMS uses the Arakawa C-grid to reduce finite-differencing error. The vertical dimension is in sigma-z coordinates, such that each layer, throughout the horizontal domain, has a constant value of σ_z:

$$\sigma_z = z_T(z - z_s)/(z_T - z_s), \tag{1}$$

where z is height (all heights are geometric relative to mean sea level), z_T is the height of the top of the model (specified as 18,400 m in this study), and z_s is the height of the local surface. Note that σ_z has units of meters, unlike other vertical coordinate systems also called sigma. However, also notice that the length of these corresponds only approximately to geometric meters, being scaled by $(z_T - z_s)/z_T$; near the surface, σ_z corresponds approximately to meters above ground level, and near the top of the model, to height above sea level.

[12] A scheme is used to allow waves impinging on the model boundaries from the inside to propagate outward

[*Klemp and Wilhelmson*, 1978a, 1978b]. A modified Kuo scheme [*Tremback*, 1990] is used to simulate subgrid-scale moist convection. The Mellor-Yamada scheme is used for vertical diffusion [*André et al.*, 1978; *Mellor and Yamada*, 1974; *Yamada and Mellor*, 1975], and a simple deformation scheme for horizontal diffusion. Information on topography and the proportion of land to water in each grid cell is fed into the model from data files.

[13] For this work, the parameterization of *Chen and Cotton* [1983, 1987] was chosen for both shortwave and longwave radiative calculations. The surface soil and vegetation parameterization of *McCumber and Pielke* [1981] and *Avissar and Mahrer* [1988] was used, with modifications as described in subsections 2.2 and 2.3. The data set of *Matthews* [1983] was used to set the vegetation types for the land surface parameterization. This work used the warm microphysics scheme for rain [*Tripoli and Cotton*, 1980] and ice microphysics for the species of snow and pristine ice crystals [*Cotton et al.*, 1982].

[14] Because RAMS version 3a was not designed as a model for climate simulation (i.e., for simulation over periods of multiple months or years), modifications were necessary. The changes fall into three categories: (1) additions specific to the Great Lakes implementation in CHARM, (2) adaptations to existing components of RAMS to make them more reasonable for use in the context of a long-term climate simulation, and (3) bug fixes. What are referred to here as ''bug fixes'' are generally parts of the RAMS 3a code that had apparently unintended consequences that may not have manifested themselves during the more routine short-term model runs. The remainder of section 2 briefly describes these changes, making reference to literature sources and the appendix for more detailed information.

2.1. Modifications Specific to CHARM

2.1.1. Time-Integrated Surface Variables

[15] For utility in the land surface and lake surface hydrology and thermodynamics formulations described later, and for diagnostic analysis, several surface variables were retained as integrals in time. These were primarily hydrologically relevant surface-atmosphere fluxes of water and energy. Those that were related to land-surface hydrology were integrated or averaged over 6-hour periods, and those used for the Lake Evaporation and Thermodynamics Model were accumulated over 24-hour periods.

2.1.2. Lake Evaporation and Thermodynamics Model (LETM)

[16] The model of lake thermodynamics used in CHARM is based on the Lake Evaporation and Thermodynamics Model (LETM [*Croley*, 1989, 1992; *Croley and Assel*, 1994]), developed at GLERL, and follows its basic formulation very faithfully. This model works on a daily time step. It uses the net shortwave and longwave radiative energy fluxes at the lakes' surfaces along with the sensible and latent heat fluxes, all of which are calculated in separate routines within CHARM and integrated over a 24-hour time period. The net amount of energy then becomes an energy input to or output from the lake. Each lake is treated as a lumped area; i.e., it is treated as having spatially constant surface temperature for purposes of determining the energy and water fluxes into the overlying atmosphere. Areal average energy fluxes are used for calculating the change in surface and subsurface water temperature with time. There is spatial variability in the energy and moisture fluxes based on the distribution of atmospheric characteristics, which is retained with regard to its effect on the overlying atmosphere.

[17] The longwave emissivity of water is taken to be 0.98. The surface albedo of water surfaces is taken to be 0.1, and for lake ice, 0.45. The surface roughness length of water and lake ice is given by the Charnock relation [*Charnock*, 1955]:

$$z_0 = \frac{0.0101}{g} U*^2, \tag{2}$$

where z_0 is the surface roughness length, g is the acceleration due to gravity (9.8 m s^{-2}), and $U*$ is the frictional velocity.

[18] The daily mean wind is used as an aging function for these daily doses or ''parcels'' of heat [*Croley*, 1989]. When heat is added to the lake during spring, it first warms the lake surface strongly, but only to a shallow depth. With time and aging (exposure to winds), this heat diffuses downward, decreasing its effect on the lake surface temperature, but increasing its influence on deeper parts of the lake. Eventually a heat parcel may fully mix to the bottom of the lake. When the lake cools again, these parcels of energy are removed, beginning with the most recent (least ''aged''). When the entire water column is cooled to 3.98°C in the fall, the water column turns over and parcels of ''cold'' begin to be added. Since 3.98°C is the temperature of maximum density of freshwater, cold water at the top of the column is stable. Complete lake turnover occurs in the spring again when the water reaches a constant temperature of 3.98°C, followed by the period of summer stratification with warm water on top. See *Croley* [1989] for a full description.

[19] As described by *Croley and Assel* [1994], ice area and thickness predictions are added to this calculation of lake temperature. Ice mass is added with the removal of energy from water already at 0°C or removed with the input of energy, with energy being converted into latent heat of fusion or of melting. Calculations of radiative, sensible, and latent heat flux are carried out separately over the ice and open water, weighting the net energy flux for each by its fractional coverage to derive an overall net heat flux into the lake.

[20] A difference in formulation from the original LETM is that the *Businger* [1966] scheme for Richardson number adjustment of bulk aerodynamic sensible and latent heat fluxes has been replaced by the *Louis* [1979] formulation, which is resident in RAMS.

[21] Some caveats are given here regarding the use of this treatment of lake thermodynamics. First, the spatial lumping of lake temperatures means that some spatially heterogeneous effects are not taken into account, chiefly the spatial distribution of lake bathymetry, which can affect its thermal properties, and the extent of the lakes into different latitudes, especially in the case of Lake Michigan. Second, the lake temperature is considered to be constant during the day, while in reality an interfacial layer can form at the surface in which mixing occurs only through molecular

diffusion, yielding strong thermal response in a very thin layer of water.

2.2. Adaptations for Climate Simulation

2.2.1. Snow

[22] A simple representation of snow was inserted into the land surface scheme of RAMS. The version of RAMS on which this version of CHARM is based had no treatment of snow. Newer release versions of RAMS include a more detailed treatment of snowpack. The present snow model component is not fully validated here. While this component conserves energy within the snowpack/soil system, its treatment of snow's effect on surface albedo is tentative and the importance of vertical distribution of temperature is not investigated.

[23] In this study, snowpack is augmented by snowfall as calculated by the ice microphysics parameterization and depleted by sublimation and melting. As soil temperature, moisture storage, and surface heat and moisture fluxes are calculated separately between the fraction of soil covered by vegetation and the bare fraction, separate accounting is also made of snowpack on the vegetated and bare fractions. For each, the fraction of land covered by snow is assumed to be the minimum of $(s/20)^{1/2}$ and 1, where s is the snow depth in millimeters water equivalent. This conceptually accounts for shallow snow occurring with spatial gaps and some effect of snow masking by vegetation. Snow is assigned an albedo of 0.45 if the air temperature at the model layer nearest the surface is above 0°C and 0.6 if it is below −10°C, with a linear relationship between these temperatures.

[24] The snow temperature is taken as equal to the temperature of the uppermost soil layer, which is 30 mm thick. As snow accumulates, its heat content and heat capacity are added to those of the top soil layer to determine an overall heat capacity and temperature. Sublimation is calculated through a bulk aerodynamic formulation similar to that used for potential evaporation from soil and vegetation [*McCumber and Pielke*, 1981; *Louis*, 1979], using the saturation vapor pressure over ice instead of that over liquid water. Evapotranspiration occurs over the non-snow-covered fraction of land, in parallel to the sublimation.

[25] Snowmelt occurs when the snow/upper soil layer reaches 0°C and additional net heat is applied to it. This net heat, the sum of the radiative, sensible, and latent (sublimation) heat fluxes exchanged with the overlying atmosphere, along with the diffusion of heat from lower soil layers, is divided by the latent heat of fusion per unit mass to derive a snowmelt rate. The snowmelt is partitioned into surface runoff and infiltrating water that is added to the moisture storage in the top layer of soil in the same manner as rainfall (see below).

2.2.2. Aggregation of Surface-Atmosphere Energy and Moisture Fluxes

[26] After being calculated for the six surface types (vegetated land, vegetated land with snow, bare soil, bare soil with snow, water, and lake ice), the upward shortwave radiation, upward longwave radiation, evapotranspiration, sensible heat flux, and momentum flux are each aggregated by averaging them, weighted by the fraction of the grid cell's area covered by each surface type. These composite fluxes then act in forcing the overlying atmosphere. This is also done in the release version of RAMS 3a, except that all land is considered snow-free and all water is considered ice-free.

2.2.3. Lowest Soil Layer Heat Capacity

[27] The soil temperature formulation within RAMS is a simple thermal diffusion model [*McCumber and Pielke*, 1981]. In the present work, the soil has 11 layers, 10 of which represent the zone between 0 and 500 mm depth, with the lowest layer below that having a thickness unspecified with regard to thermal characteristics. Under the release version of RAMS 3a, the lowest layer is initialized to and permanently held at a specified temperature. This was changed to allow for temporal variability in the temperature of that lowest layer, with the lowest soil layer acting as a simple thermal pool with a specified heat capacity. A theoretical justification for the choice of that heat capacity is presented in Appendix A.

2.2.4. Lowest Soil Layer Water Percolation

[28] The assumption built into RAMS version 3a, that no water percolates through the bottom of the lowest soil layer, is replaced with the assumption that percolation occurs in accordance with the soil moisture content of the lowest soil layer and the equations of *Clapp and Hornberger* [1978] [see also *McCumber and Pielke*, 1981]. Only the gravity-based water drainage is used, not vertical diffusive soil moisture transport. This water enters the groundwater reservoir of the Large Basin Runoff Model (LBRM, similar to *Croley* [1983]), and is no longer available for evapotranspiration.

2.3. Modifications to Solve Specific Problems

2.3.1. Numerical Stability of the Boundary Layer Formulation

[29] The RAMS option for Mellor-Yamada type turbulence closure in the boundary layer was used [*André et al.*, 1978; *Mellor and Yamada*, 1974; *Yamada and Mellor*, 1975]. This scheme requires prognostic determination of the turbulent kinetic energy, but the numerical scheme for this can become unstable at the lowest model level when the turbulent kinetic energy reaches high values. The prognostic equation for turbulent kinetic energy is of the following form:

$$\frac{\partial E_{TK}}{\partial t} = B - CE_{TK}^{3/2}, \tag{3}$$

where E_{TK} is the turbulent kinetic energy, B at the lowest model level is proportional to the wind speed, and C at the lowest model level is approximately $1/(5.87\,\kappa z_r)$, where κ is von Kármán's constant (taken as 0.35) and z_r is the height above the ground of the lowest model level. The ordinary forward difference form of this would be

$$E_{TK}^{t+1} = E_{TK}^{t} + \left[B - C\left(E_{TK}^{t}\right)^{3/2}\right]\Delta t, \tag{4}$$

with Δt being the length of the time step and superscripts indexing the time step. To correct occasional numerical instability when using this form, however, equation (3) is partially linearized in E_{TK}, and solution is found in the form of exponential functions. That is, $E_{TK}^{3/2}$ was split into factors of E_{TK} and $E_{TK}^{1/2}$; E_{TK} was assumed to be variable and $E_{TK}^{1/2}$ to be constant over the time step (a better approximation than

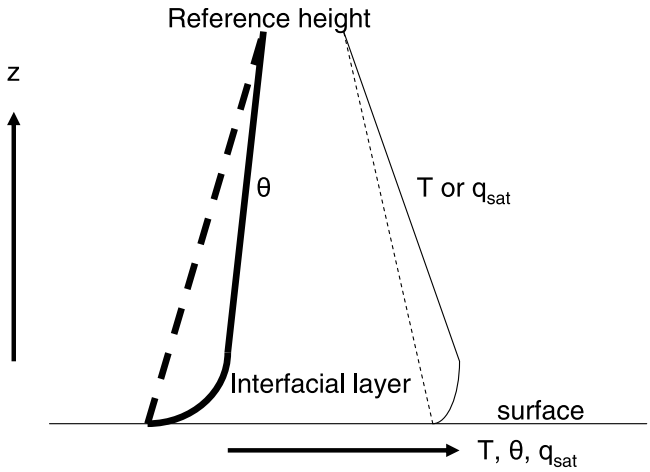

Figure 1. Schematic depiction of the case in which the gradient of potential temperature and in situ temperature between the surface and reference height are of opposite sign. Because saturation mixing ratio is a monotonic function of air temperature, temperature can be used as a proxy. The solid curves illustrate a realistic schematic profile at heights intermediate between the surface and reference height, while the dashed lines illustrate the assumption of linear interpolation with height.

that implicit in (4), that $E_{TK}^{3/2}$ is constant over the time step). From this is derived a form that aids in maintaining numerical stability:

$$E_{TK}^{t+1} = E_{TK} + \left(1 - e^{-CE_{TK}^{1/2}\Delta t}\right)\left(\frac{B}{CE_{TK}^{1/2}} - E_{TK}\right), \qquad (5)$$

where all instances of E_{TK} on the right-hand side of the equation use the value for time step t. Although the limit of this solution as C, E_{TK}, or Δt approaches zero is equation (4), the form in (5) is useful for maintaining numerical stability when these values, particularly E_{TK}, become large. The problem addressed by this reformulation has been solved in later release versions of RAMS by using a time-split scheme in calculating vegetation temperature.

2.3.2. Elimination of Evapotranspiration With Supersaturated Atmosphere

[30] Another correction was to severely curb surface evapotranspiration whenever the lowest layer of the model becomes supersaturated. The release version of RAMS 3a simply assumes that monotonic gradients of water vapor mixing ratio and potential temperature exist between the surface and the reference height. As illustrated schematically in Figure 1, it is not uncommon to have a small negative gradient of potential temperature θ between the surface and the reference height (Δθ defined as $\theta_{surface}$ minus θ_{ref}) while the gradient of in situ temperature T is positive, since

$$\Delta\theta = \Delta\left[T\left(\frac{p_0}{p}\right)^{2/7}\right] = \left(\frac{p_0}{p}\right)^{2/7}\left(\Delta T - \frac{2T}{7p}\Delta p\right). \qquad (6)$$

In (6), p_0 is reference pressure defined as 1000 mb, p is local pressure averaged between the surface and reference height, and Δp is surface pressure minus reference height pressure (a positive definite quantity). If the Δp term on the right-hand side of (6) is of greater magnitude than the ΔT term (i.e., if ΔT is small enough), ΔT and Δθ will be of opposite sign. T also serves as a proxy for saturation mixing ratio in the schematic of Figure 1, and therefore it is possible to predict evapotranspiration in the presence of a supersaturated reference height, even though the reference level potential temperature is greater than the surface potential temperature. The result is that latent heat flux can be partially sustained by sensible heat flux in the opposite direction.

[31] Figure 1 also shows more realistic schematic profiles of θ and T (proxy for q_{sat}) at heights intermediate between the surface and reference height. The sharpest gradient in θ occurs in the interfacial layer immediately above the surface, thus forcing the local gradient of T to have the same sign as the gradient in θ, and only a small gradient in θ above the interfacial layer. The modification implemented in CHARM is that, under conditions of supersaturation of the lowest model layer (fog), for purposes of calculating evapotranspiration, the reference level mixing ratio is taken to be that of a parcel that has been adiabatically moved from the reference level to immediately above the surface, and then saturated with water vapor. This is intended to represent a saturated parcel located at the top of the interfacial layer, but the practical effect of this is to eliminate evapotranspiration under the condition of a saturated lowest model level and stable potential temperature gradient between the surface and reference height. This procedure has some effect on reducing the frequency and persistence of low-level cloud decks.

2.3.3. Greater Precipitation Infiltration

[32] Another modification was to allow greater infiltration of precipitation into the ground. The formulation for infiltration built into RAMS takes runoff as precipitation multiplied by the mean saturated fraction of the top 60 mm (two model layers) of soil. The gravity-driven soil percolation rate, on the other hand, was taken as proportional to the saturated fraction raised to a soil type-dependent exponent, as in *Clapp and Hornberger* [1978], with these exponents ranging from 11.1 to 25.8. Because of these large exponents, it happens frequently that the top 60 mm of soil nears saturation sufficiently to prompt much surface runoff, while very little percolation occurs below that level. This tends to keep all but the uppermost soil dry and may be expected to curtail evapotranspiration, instead enhancing runoff.

[33] To make these formulations more consistent, surface runoff was made equal to the precipitation multiplied by the saturated fraction of the top 60 mm of soil raised to the same power as in the formula for gravity-driven percolation. This is supplemented by a provision that enough runoff occurs to prevent the uppermost model layer (30 mm) from exceeding its saturation point. Together, these provisions yield slightly more runoff than an infiltration exceedance formulation: a saturated top soil layer indicates that there is more water impinging on it than can be percolated through the soil, so the excess becomes runoff. There can be some additional runoff, but it can only be substantial when the top two soil layers are quite close to saturation. Most of the results presented in this paper use this modified formulation, but the last part of section 5 describes an experimental

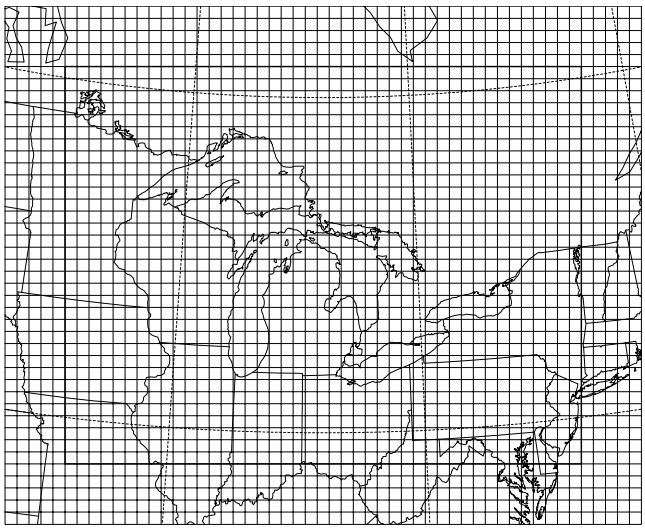

Figure 2. Map of the CHARM domain. The light lines indicate the grid boxes of the model: 40 km spacing with 53 grid points in the x direction (approximately east-west) and 43 grid points in the y direction (approximately north-south). The heavy lines indicates the boundary between the outer domain, in which the atmospheric state variables are nudged toward the NCEP Reanalysis values, and the inner domain, in which the variables are nudged only at the uppermost vertical levels. Unless otherwise indicated, data shown in all succeeding figures are from the inner domain only.

comparison to the results with the old formulation, with increased surface runoff and lower infiltration.

2.3.4. Removal of Linearization of Equation of Vertical Motion

[34] As detailed in Appendix B, RAMS has used a version of the equation of vertical motion that has been linearized, resulting in a modified definition of the hydrostatic state. An additional experimental run was executed with a corrected nonlinear formulation, with results described in section 4.

3. Experimental Design

[35] CHARM is run for a 2-year period (calendar years 1993 and 1994) on a stereographic grid encompassing the entire Great Lakes drainage basin, with 53 grid points in the x-direction and 43 in the y-direction, spaced at 40 km intervals (Figure 2). The center of the domain is at 45°N, 84°W. There are 22 vertical levels, with the lowest above the ground being 100 m thick (in sigma-z coordinates, thus in most nonocean grid points slightly less than 100 m), and each successive interval thicker by a factor of 1.2, up to a maximum of 1900 m thick in sigma-z coordinates. The model top is a rigid lid at 18,400 m above mean sea level.

[36] National Centers for Environmental Prediction (NCEP) Reanalysis data [*Kalnay et al.*, 1996] are used as initial and lateral boundary conditions. The lateral boundary conditions are imposed using a nudging scheme. The pressure, wind velocity vector, temperature, and water vapor mixing ratio are relaxed toward the NCEP Reanalysis data with a time constant of 120 min at the outermost grid row. The coefficient of relaxation (reciprocal of the time constant) is reduced linearly to zero through the outermost five grid rows (outside of the heavy box in Figure 2). The same quantities are relaxed to observed values with a time constant of 30 min at the top model level, with the relaxation coefficient reduced linearly to zero at 12,500 m (in sigma-z coordinates).

4. Validation of Atmospheric Variables

[37] The monthly mean bias in CHARM's modeled air temperature at the lowest model level varies by season (Figure 3). The outermost five grid rows in the domain (outside the heavy box in Figure 2) are nudged using prescribed lateral boundary conditions and have been omitted from the calculations used to create all of the figures, except where indicated by ''full domain'' or ''outer domain.'' In the inner domain (excluding the five outermost grid rows), there are positive near-surface air temperature biases during the winter, and negative biases during the summer, and an annual mean bias in 1994 of −0.68 K.

[38] On a spatially decomposed basis, these biases take on some characteristics that are correlated with the location of the lakes. During January there is generally warmer air over the lakes in the model than in neighboring regions (Figure 4a). This is far less evident in the data directly interpolated from the NCEP Reanalysis data (Figure 4b), but is in evidence in the interpolation from ground stations (Figure 4c). Note particularly the warmer air observed over the eastern part of Lake Michigan and over the land just to its east. Unfortunately, the availability of near-surface temperature data over Lakes Superior and Huron make validation on this point more difficult.

[39] During July a warm air signature somewhat surprisingly remains over the lakes (Figure 5a). This signature is even evident in the interpolated reanalysis data (Figure 5b), where it is likely caused by the topographic features that surround Lake Ontario and eastern Lake Erie. That is, interpolation is done on the potential temperature, so that if the lakes have similar potential temperature to surrounding land areas but lower elevation, their in situ temperature will be higher. CHARM's cold bias relative to surface observations (Figure 5c) is especially evident over the higher elevation regions near the eastern Great Lakes, and to a lesser degree in the rest of the southern part of the inner domain.

[40] Figure 6 shows profiles of temperature biases on a plane representing height and the model x-coordinate (corresponding closely to longitude), averaged in the y-direction within the model's inner domain. In January 1994 (Figure 6a), the near-surface temperature has a rather strong positive temperature bias, as was indicated in Figure 4. The strongest temperature biases are confined to the lowest 1 km of the atmosphere. Above this height, the temperature bias is less than 1 K.

[41] With the prevailing wind from the west during January, the temperature (Figure 6a) near the western edge of the inner domain is much more strongly influenced by the input from the NCEP Reanalysis data. At levels below 1 km near the western edge of the inner domain, the temperature bias is noticeably less than in the interior and eastern edge of the inner domain.

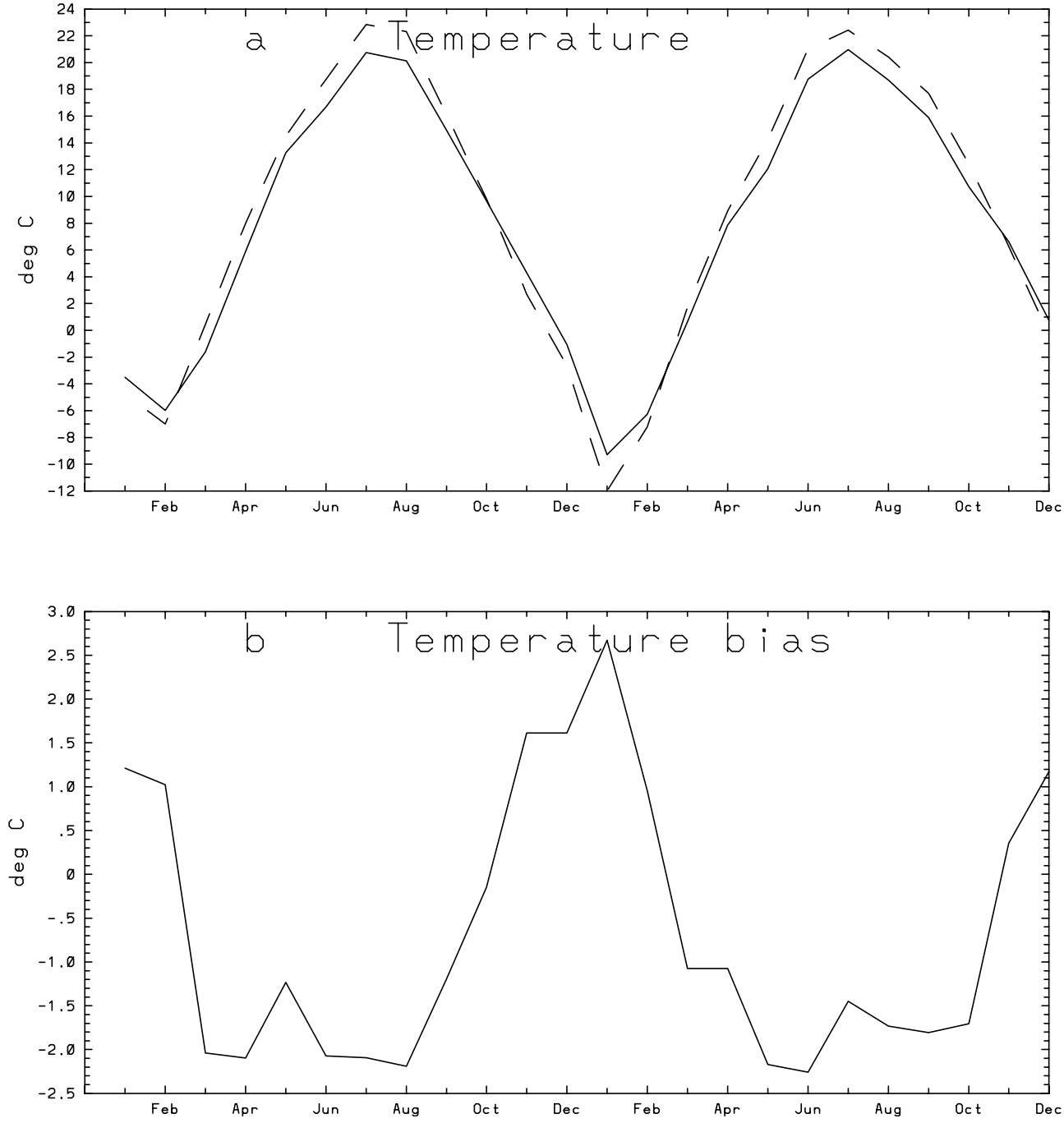

Figure 3. (a) Monthly mean temperature in the lowest model layer (°C) for CHARM (solid curve) and NCEP Reanalysis data (dashed curve), which were also used as lateral boundary conditions for the model runs. (b) Temperature bias (CHARM minus NCEP Reanalysis). Values are areally averaged over the inner domain (see Figure 2).

[42] Figure 6b shows a rather different spatial configuration of temperature biases during July 1994. There is a general negative temperature bias, with its maximum magnitude not adjacent to the surface, but elevated. The largest negative temperature biases occur at just under 1 km above mean sea level. This phenomenon is believed to be due to excessive stratus cloud cover, with cloud tops near this level losing heat radiatively. Similarly, in Figure 6a, a minimum in the positive temperature bias is situated at a slightly higher level, also likely due to radiative loss from frequent dense stratus clouds. Additional implications of this cloud cover in terms of solar radiative flux at the surface will be discussed later in this section.

[43] For purposes of comparison of precipitation amounts, Summary of Day data from surface stations were acquired from the Midwest Regional Climate Center and mapped onto the CHARM grid points using inverse distance weighting, for those grid points that were within 40 km of a station. There is a qualitative match between the observed and simulated peaks and troughs in monthly

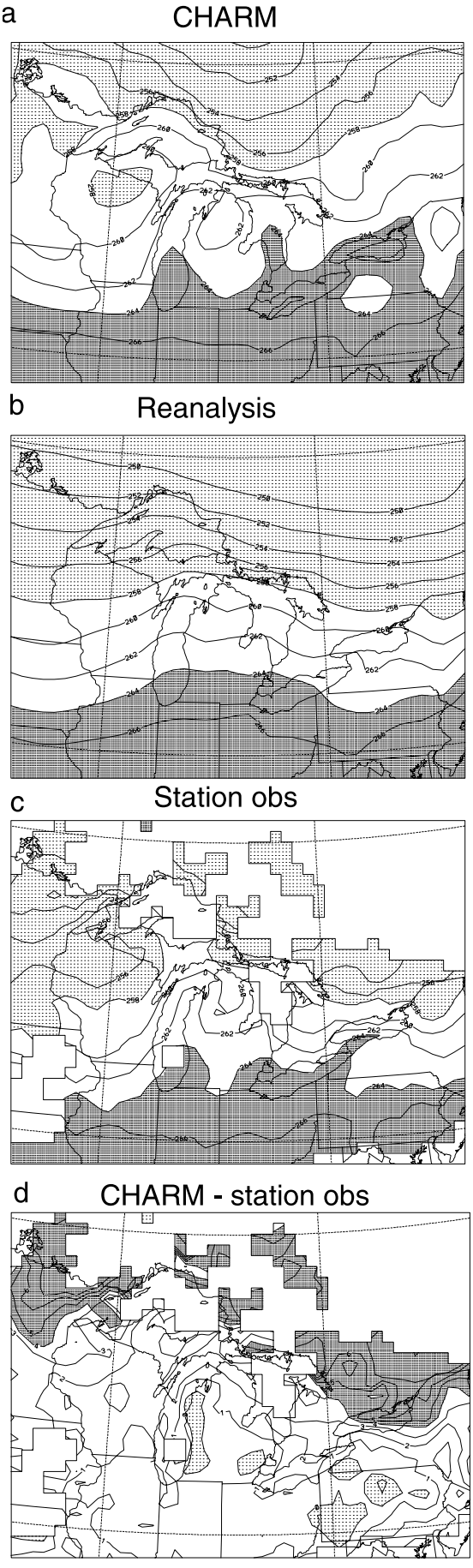

precipitation rates (Figure 7a). However, precipitation generally has a positive bias during winter and early spring and a negative bias during the summer and into the fall (Figure 7b). As summer is the season of highest precipitation rates, although the negative summer precipitation biases are smaller in percentage terms, they largely offset the positive biases during the winter. This produces a relatively small annual mean bias; for 1994, the annual mean precipitation, averaged over the inner domain, was excessive by 1.88 cm, or 6.6%.

[44] The spatial distribution of annual precipitation shows reasonable agreement between observations and simulation (Figure 8). The simulation captures, but exaggerates, the general eastward gradient of total precipitation amounts. In particular, it underpredicts precipitation on the western margin of the domain. Because the prevailing wind is from the west, particularly during winter, this seems to indicate that there is a transition zone within which air entering the model domain is adjusting to the conditions consistent with the interior domain of CHARM before achieving the conditions in which precipitation would form. It also seems that, at least in this case, the air in this western part of the domain is largely untouched by uplift that could lead to precipitation.

[45] The model also exhibits stronger small-scale structure than the observations, even though the observations were taken from 1788 stations. It is encouraging that several localized maxima are realistically located, namely, the belts of lake-effect precipitation: just east of Lake Superior (in the form of a maximum axis in the model, not a ''bull's-eye''), east of Georgian Bay, on the southeastern perimeter of Lake Erie, and east of Lake Ontario on the rise into the Adirondack Mountains. Unfortunately, the magnitude of each of these centers of precipitation is exaggerated by the model. Also, the position of the lake-effect band east of Lake Michigan does not agree between the model and observations.

[46] One notable problem is a tendency toward unrealistically low mean sea level pressure and geopotential heights at various pressure levels (Figures 9, 10, and 11a). Apart from the overall biases toward low sea level pressure, CHARM replicates the generalized center of low pressure over the Great Lakes during January, adding details that appear to be thermally driven pressure patterns associated with the individual lakes (Figure 9). Although averaged over a month-long period, these results are consistent with the findings of *Sousounis and Shirer* [1992] and *Sousounis and Fritsch* [1994] regarding lake-aggregate low-pressure systems. The pressure gradients in the northwestern corner

Figure 4. Temperature of the lowest model layer (~50 m above ground level) during January 1994 (a) as simulated by CHARM, (b) as interpolated from the NCEP Reanalysis data to the CHARM grid, (c) interpolated from surface station observations, and (d) CHARM simulation minus station observations. In Figures 4a, 4b, and 4c the contour interval is 2 K; light shading indicates temperatures below 258 K, and dark shading indicates those above 264 K. In Figure 4d the contour interval is 1 K; light shading indicates values below 0 K, and dark shading indicates those above 4 K.

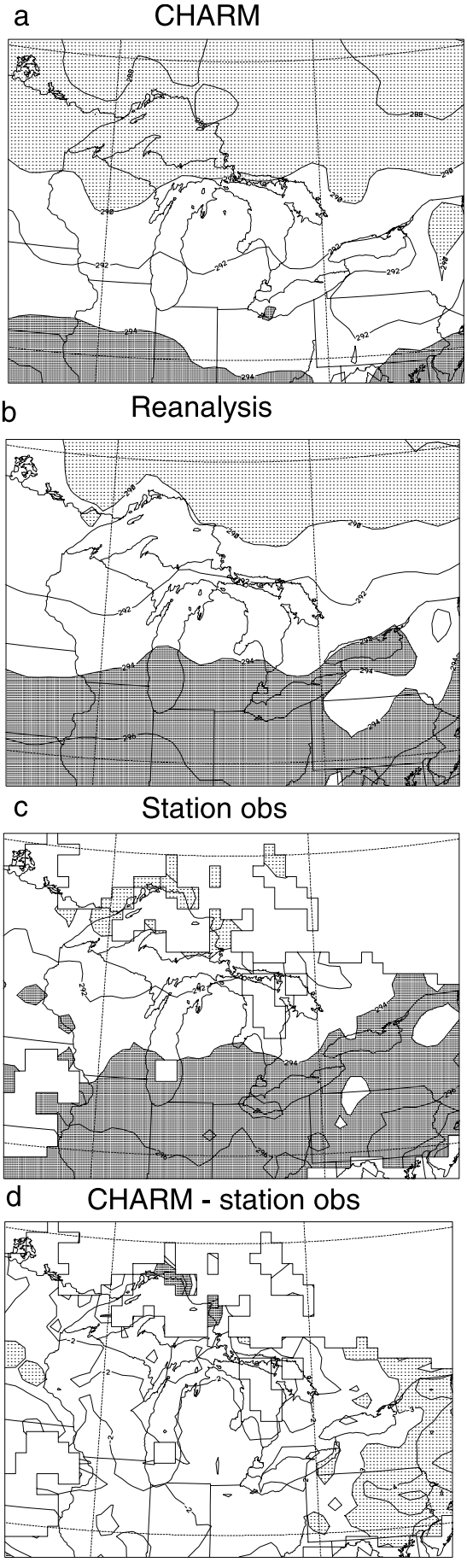

Figure 5. As in Figure 2, but for July 1994. In Figures 5a, 5b, and 5c the contour interval is 2 K; light shading indicates temperatures below 288 K, and dark shading indicates those above 294 K. In Figure 5d the contour interval is 1 K; light shading indicates values below −3 K, and dark shading indicates those above 0 K.

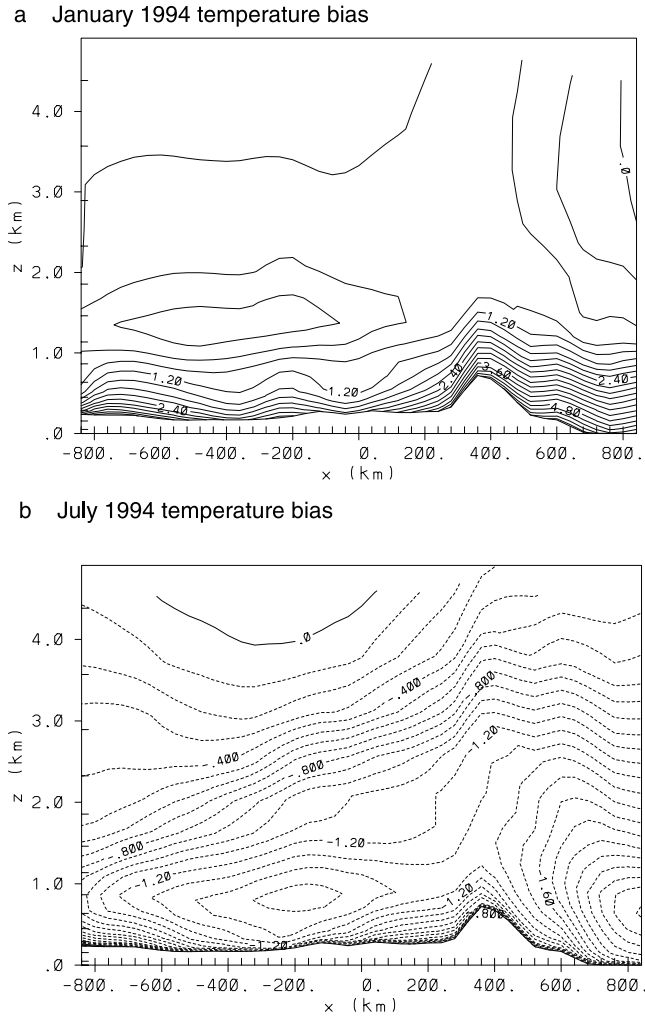

Figure 6. Temperature bias (simulated minus NCEP Reanalysis) for (a) January 1994, with contour interval of 0.3 K and (b) July 1994, with contour interval of 0.1 K. The ordinate is height above mean sea level, and the abscissa is in units of kilometers in the x-direction (roughly east-west) in CHARM's native stereographic projection, relative to the domain's center at 45°N, 84°W. Values are averaged in the y-direction (roughly north-south) over the inner domain (the portion that is not relaxed toward observed values).

of the inner domain and near and extending east from Lake Ontario are excessively strong.

[47] During July the strength of the pressure gradients is in good agreement between CHARM and the reanalysis data (Figure 10). However, the isobars for CHARM (Figure 10a) in the eastern part of the domain are rotated counterclockwise relative to those from the reanalysis data.

[48] The area-averaged geopotential height biases at 1000, 700, 500, 300, and 200 hPa are all shown in

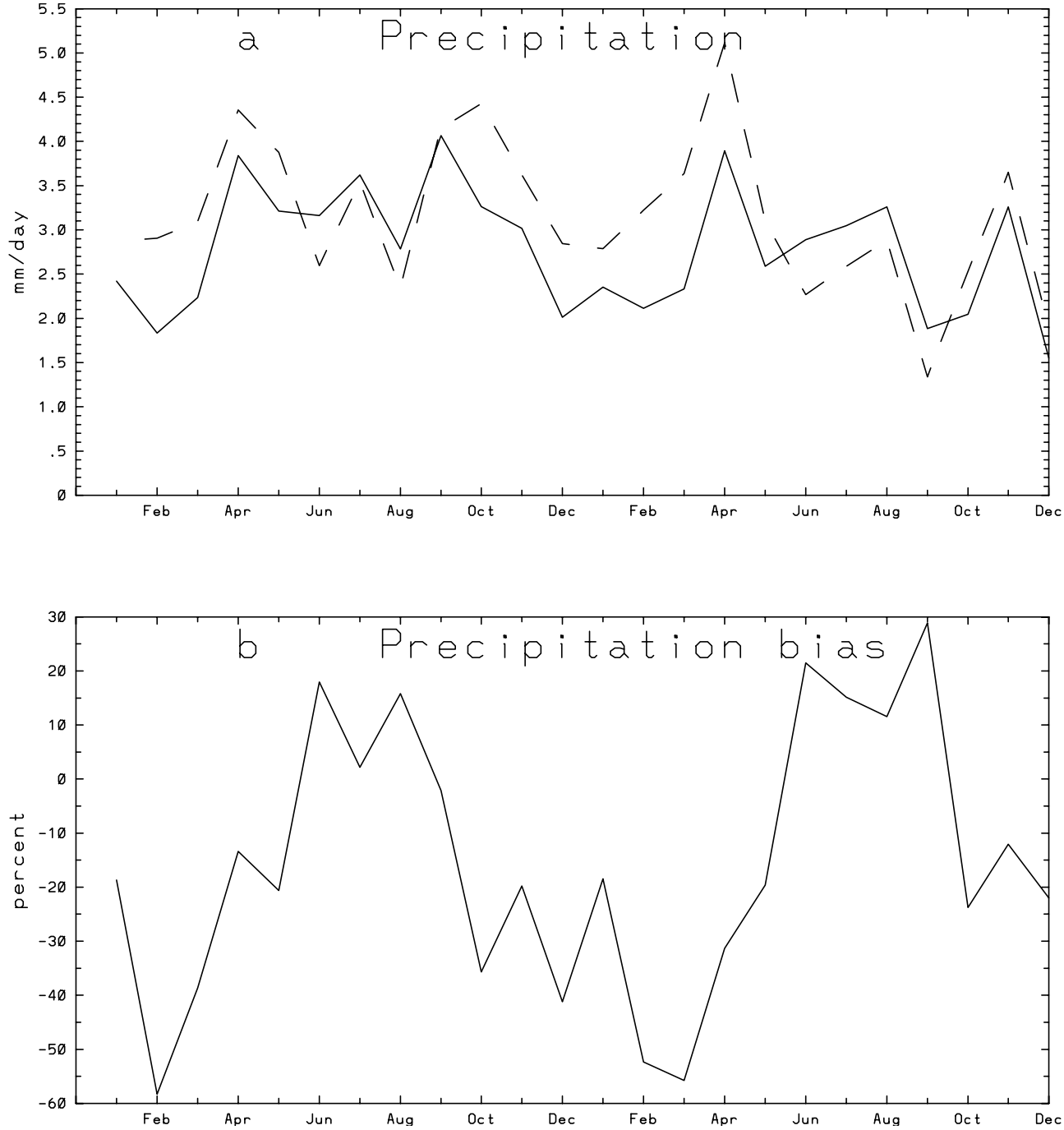

Figure 7. (a) Monthly mean precipitation (millimeters per day) interpolated from station observations at grid points within the inner domain with a station within 80 km (dashed curve) and CHARM-simulated precipitation at the same set of grid points (solid curve). (b) Percent precipitation bias (CHARM minus interpolated station observations) over the same set of points.

Figure 11a, in order to demonstrate their similarity, indicating that the low-pressure bias is not an entirely baroclinic phenomenon and should not be expected to be only due to temperature anomalies in the atmosphere. Additionally, Figure 6 shows a lack of the deep, large-magnitude temperature biases required to create baroclinically generated pressure or geopotential height biases.

[49] Finally, an additional model run was carried out, and is labeled as the ''corrected'' run in Figure 11b. It is corrected in the sense that RAMS's standard linearized version of the equation of vertical motion is replaced by the full form of the equation. This also results in a change in the definition of the normally expected hydrostatic state of the vertical column. For details on the correction to the formulation, see Appendix B. The correction yields its most prominent change during the winter months, further reducing what baroclinic character there is to the geopotential height anomalies (compare Figures 11b and 11a).

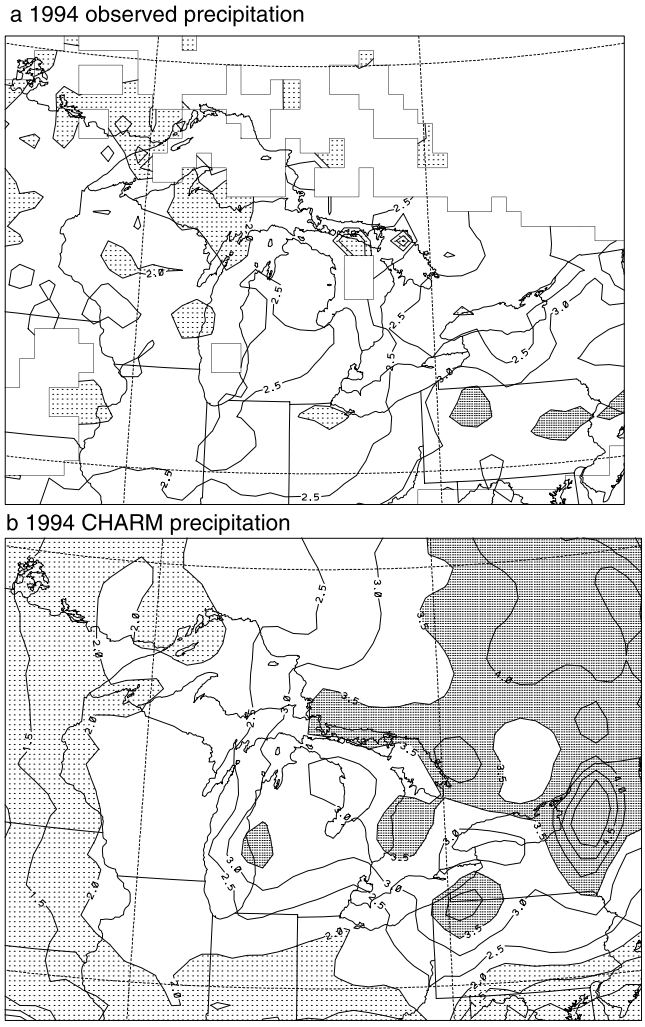

Figure 8. (a) Observed precipitation for 1994, interpolated from station observations, with blank areas indicating no stations within 80 km, and (b) 1994 precipitation simulated by CHARM. The contour interval is 0.5 mm day^{-1}, with light shading for less than 2 mm day^{-1} and heavy shading for greater than 3.5 mm day^{-1}.

[50] Instead of pressure biases being due to temperature-related baroclinic effects, there appears to be a correlation between the monthly mean geopotential height biases and the divergence of air from the outer part of the domain. This is shown as simulated by CHARM and as in the NCEP Reanalysis data in Figures 11c and 11d, respectively. These figures show the divergence of the volumetric mass transport vector (i.e., the wind vector multiplied by the air density), vertically integrated over the column up to 18400 m, the maximum height that was simulated. The Divergence Theorem was used to calculate this using a contour integral along the edges of the entire model domain and the edges of the inner domain. Comparison to Figures 11a and 11b shows that the area-averaged (over the inner domain) mean sea level pressure has intermonthly variations that are correlated to the difference in the mass transport divergence between the inner domain and the entire domain. For example, there is a minimum in geopotential heights in April, when the inner domain is highly convergent and the entire domain is divergent. Conversely, geopotential height is biased high in September, when the inner domain is divergent and the entire domain is convergent. This difference in divergence (more precisely, entire domain divergence multiplied by the area of the entire domain minus inner domain divergence multiplied by the area of the inner domain, divided by the area of the five grid rows around the edge of the domain) represents the air divergence from the outer five grid rows of the entire domain.

[51] The month-to-month variations of divergence over the entire domain correspond well between the observations and CHARM. However, CHARM has an overall bias toward positive divergence relative to the observations. Over the inner domain, the intermonthly variations do not correspond as closely, and CHARM is biased toward convergence relative to the observations. The modeled divergence compares closely between the original and corrected model runs (Figure 11d).

[52] The reason why the modeled divergence tends to be positive over the entire domain and negative over the inner

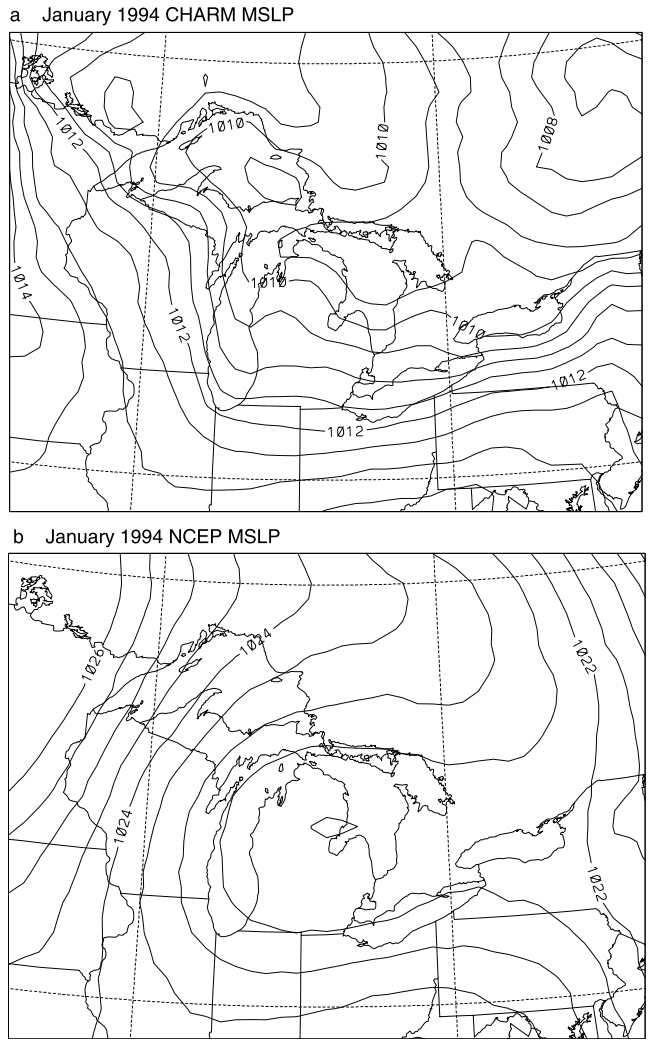

Figure 9. Mean sea level pressure averaged over January 1994 from (a) CHARM and (b) NCEP Reanalysis data interpolated to the CHARM grid. The contour interval is 0.5 hPa.

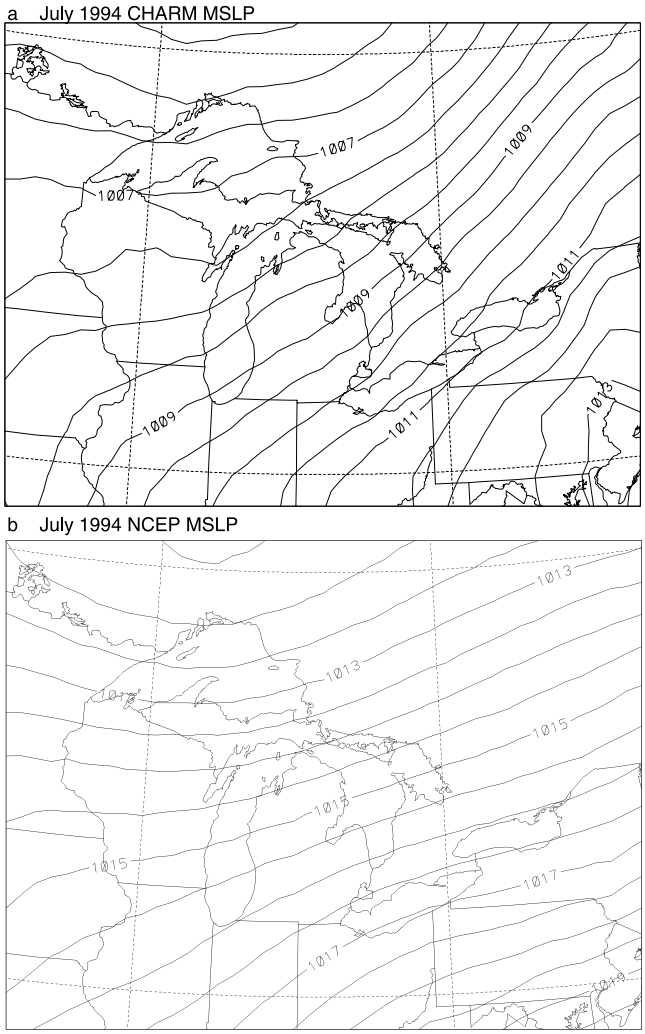

Figure 10. Same as Figure 9, but for July 1994.

domain, indicating strong divergence in the lateral boundary region of the domain, is unknown. Many guesses are possible, but have not been fully investigated, such as topographic effects, the handling of wave propagation out of the domain, winds associated with convective precipitation which concentrates near the edges of the inner domain, or the analysis of the lateral boundary condition input onto CHARM's three-dimensional grid.

[53] Corresponding to the pressure patterns of Figure 9, CHARM has stronger near-surface winds during January in some areas than does the reanalysis data (Figure 12). The grossest features of the wind field are consistent with the geostrophic relationship, but, as one would expect near the surface and especially near sources of mesoscale thermal

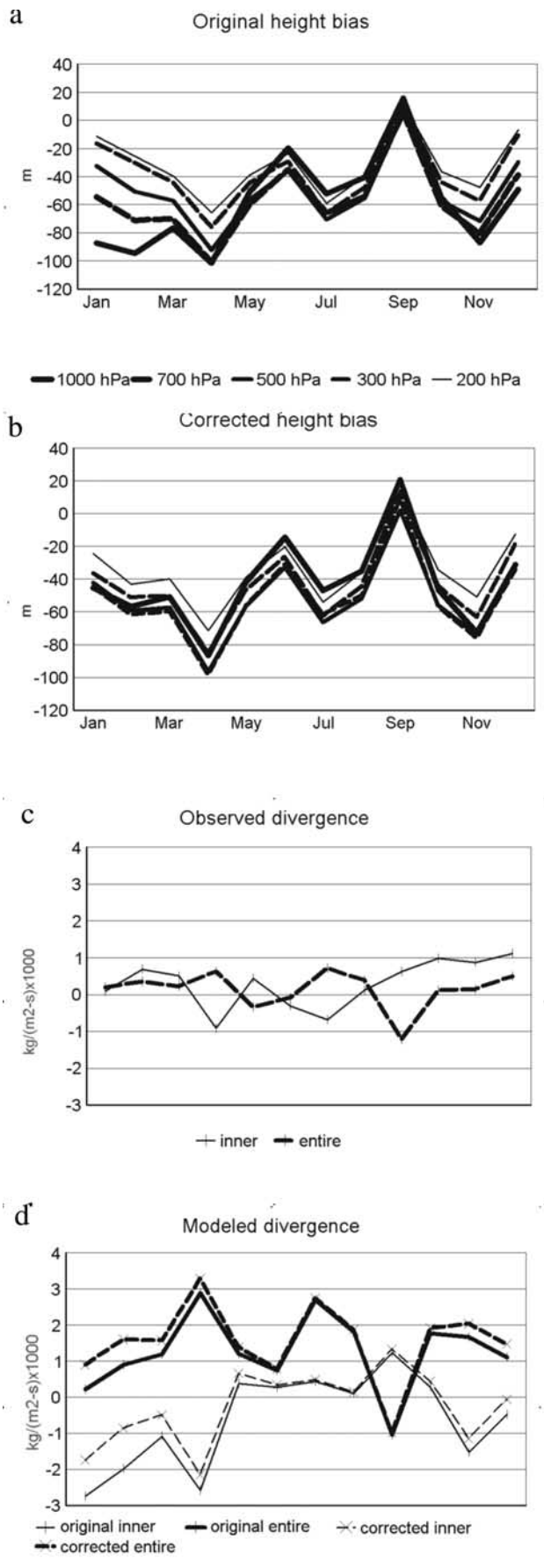

Figure 11. (a) Geopotential height bias in the original model run (model - observed, in meters) and (b) in the corrected model run (see Appendix B) during all months of 1994 at various pressure levels over CHARM's inner domain; and (c) vertically integrated mass flux divergence (kg m^{-2} s^{-1}) averaged over the inner and entire domain for the NCEP Reanalysis data used as input to CHARM and (d) CHARM output.

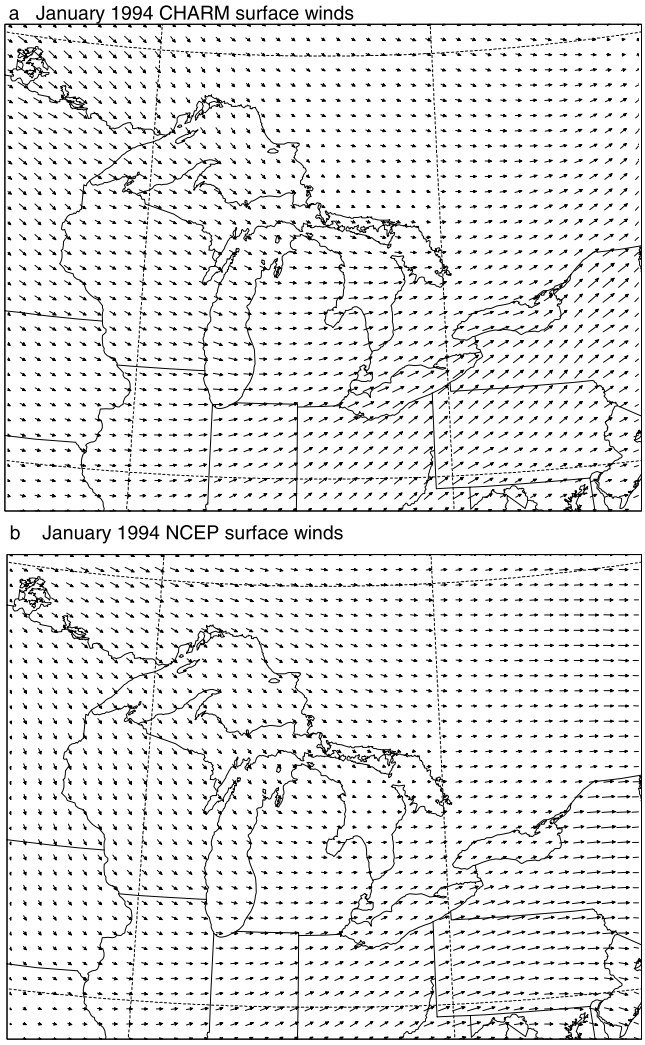

Figure 12. Mean wind vectors from the lowest model level for January 1994 from (a) CHARM and (b) NCEP Reanalysis data interpolated to the CHARM grid. The vectors are scaled such that the distance between the tails of adjacent arrows is equal to 7 m s^{-1}.

forcing, geostrophy is not followed in detail. In particular, the features in the pressure distribution at scales smaller than the entire domain are not strongly reflected in the monthly mean wind field, especially in the CHARM output, but also in the NCEP Reanalysis data. Likewise, the July winds (Figure 13) reflect the surface pressure patterns of Figure 10, in having a greater southerly component in the eastern part of the domain. The magnitude of the winds during July is in greater agreement between CHARM and the NCEP Reanalysis than in January.

[54] The mean surface net solar radiation simulated by CHARM during 1994 (Figure 14a) is much less than that derived by the Surface Radiation Budget project (Figure 14b, derived from *Pinker and Laszlo* [1992], acquired from http://charm.larc.nasa.gov/GUIDE/dataset_documents/srb.html). In many areas it is less than half as much. While the net solar radiation is higher in the western and southern extremes of the inner grid and directly over the Great Lakes than elsewhere, the bulk of the domain is regularly covered by thick and persistent stratus cloud decks. These are explicitly predicted using the microphysics scheme that is enabled here. This is in contrast to *Liston and Pielke* [2001], who used a radiative formulation that ignores clouds. Experimental use of this formulation (not shown here) reveals the opposite problem: excessive net solar radiation at the surface and year-round positive air temperature biases near the surface. This excessive cloudiness is a likely cause of the biases noted from Figures 2, 3, and 4: near-surface air temperatures are too low during the summer, when the reflectivity of the clouds has the dominant effect, and too high during the winter, when the greenhouse effect exerted by the clouds gains dominance.

[55] That the low values of net surface radiation are due to low-level clouds associated with excessively moist near-surface air is supported by Figures 15 and 16, which show the water vapor mixing ratio of the lowest model level for January and July 1994, respectively, along with the difference from the NCEP Reanalysis values. One likely mechanism is pointed to by Figure 15b, which shows a strong positive bias in mixing ratio near the chain of inland

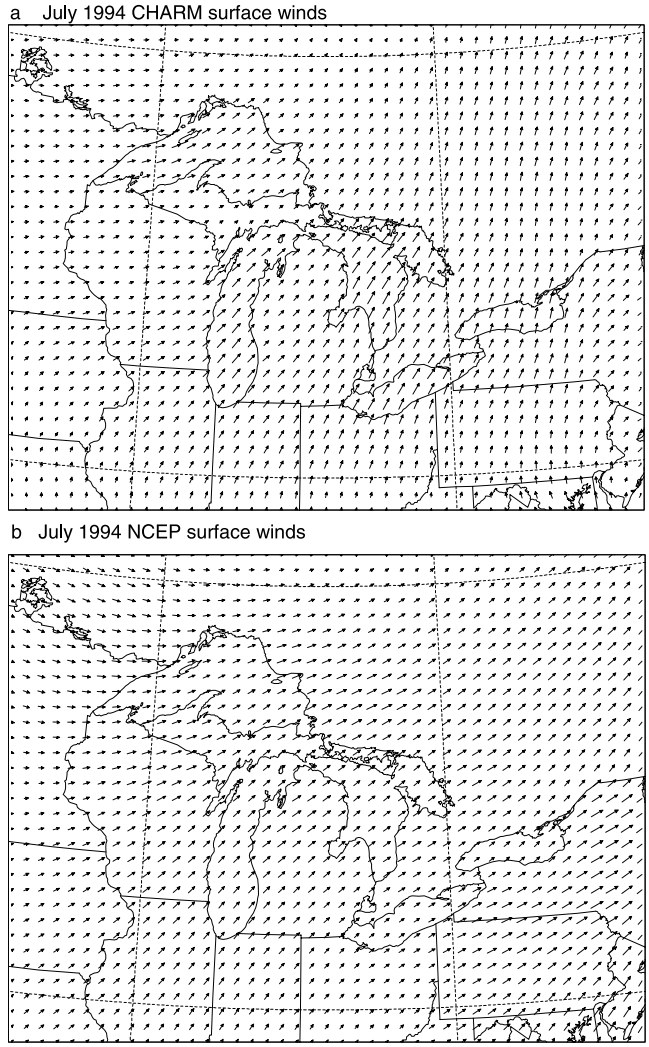

Figure 13. As in Figure 12, but for July 1994. The vectors are scaled such that the distance between the tails of adjacent arrows is equal to 5 m s^{-1}.

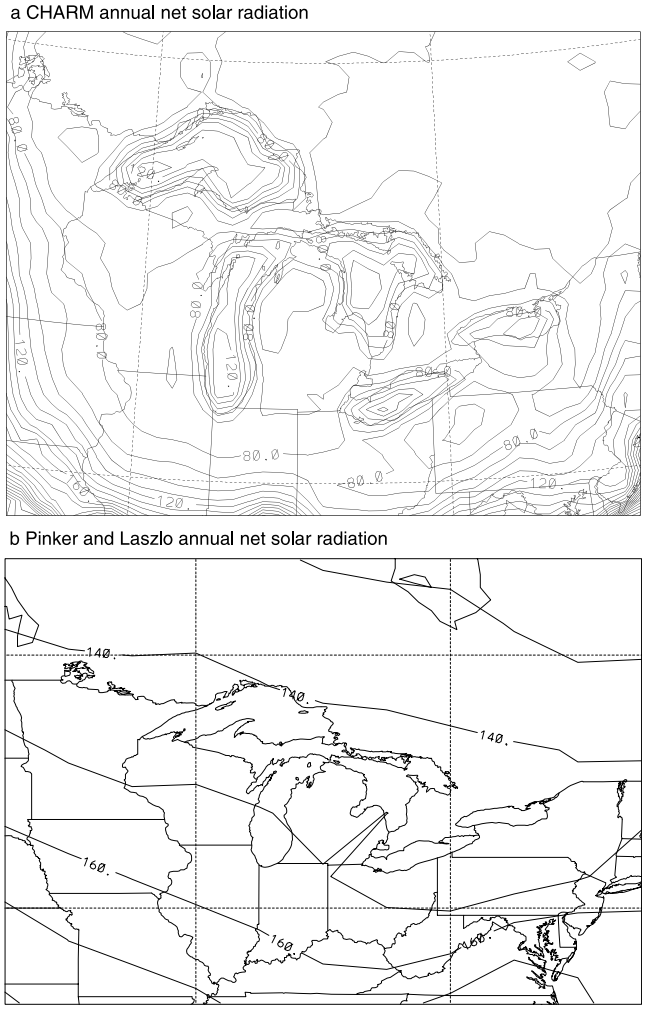

Figure 14. (a) Simulated 1994 annual mean net solar radiation in W m^{-2} and (b) observed net solar radiation from the Surface Radiation Budget program [*Pinker and Laszlo*, 1992].

lakes extending to the west of Lake Superior, and also in the northeastern part of the domain, which has many inland lakes as well. In model grid boxes that are located outside of the Great Lakes drainage basin, the surface temperature for the fractional area that is assigned to water is taken as a spatial interpolation of ocean temperatures given by the *Reynolds* [1988] sea surface temperature climatology. During the winter, these temperatures are unrealistically high for inland lakes, mainly because of the high heat capacity of the oceans relative to inland lakes, with local climate and altitude also acting. The unrealistically warm inland lakes act as strong water vapor sources, unaffected by energy budget limitations. Mitigating this assertion of the cause of excessive humidity is the fact that Figure 15b shows the strongest positive biases in mixing ratio in the extreme southeastern corner of the inner domain, over the ocean, where the *Reynolds* [1988] data should be reliable. Given this, it should also be remembered that the NCEP Reanalysis data represents values averaged over areas 2.5 degrees on a side, with the values shown here representing spatial interpolations of those data. During July (Figure 16) the water vapor mixing ratio has its largest positive bias in the southwestern part of the domain, and the biases are reduced over Lakes Superior, Michigan, and Ontario relative to surrounding areas.

5. Validation of Hydrologic Variables

[56] While the previous formulation of surface runoff, as described in subsection 2.3.3, produced much surface runoff and little infiltration into the soil, the new formulation produces much water drainage through soil percolation and little surface runoff. Following the concepts of *Croley* [1983], this would imply that the great bulk of the water is transferred to groundwater storage, with very little going directly to surface water storage, such as inland lakes, ponds, and rivers. The water routed to surface storage would be expected to drain to the Great Lakes on short timescales relative to the water stored in the ground. A main goal of the

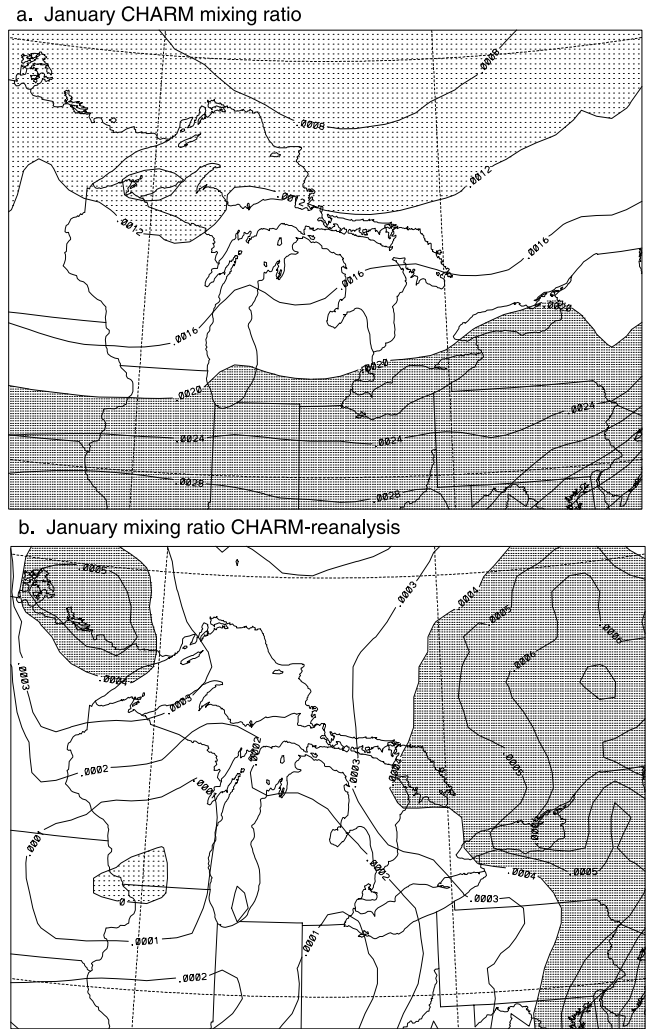

Figure 15. (a) January 1994 water vapor mixing ratio at the lowest model level for CHARM, with contour interval of 0.0004, dark shading for values greater than 0.002, and light shading for values less than 0.0012; and (b) for CHARM minus NCEP Reanalysis, with a contour interval of 0.0001, dark shading for values greater than 0.0004, and light shading for values less than 0.

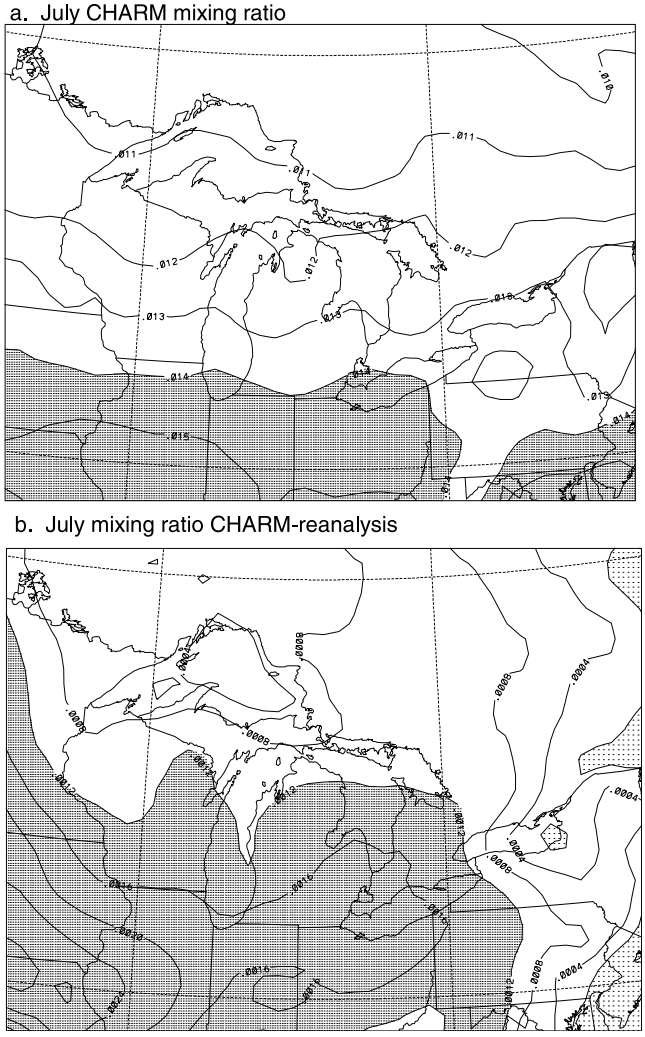

Figure 16. (a) July 1994 water vapor mixing ratio at the lowest model level for CHARM, with contour interval of 0.001 and dark shading for values greater than 0.014; and (b) for CHARM minus NCEP Reanalysis, with a contour interval of 0.0004, dark shading for values greater than 0.0012, and light shading for values less than 0.

hydrologic portion of this overall project (not yet reached in the work presented in this paper) is to gauge the long-term net basin supply of water to the Great Lakes and anticipate mean changes in the Great Lakes' water levels due to climatic forcing. However, because runoff of tributary streams is a more responsive variable than lake level at timescales less than a year or so, validation of runoff will concentrate on the sum of surface runoff and the water percolated through the active soil layer, compared to stream gage data for the drainage subbasins. A likely future effort will be to use empirical fitting of the partitioning between surface runoff and soil water percolation to groundwater and some parameters for delaying the water drainage into the Great Lakes, in order to mimic the observed temporal characteristics of the flow in rivers tributary to the Great Lakes.

[57] The runoff totals in the Lake Superior and Lake Michigan drainage basins are presented in Figure 17. The modeled values, representing the monthly sum of surface runoff and percolation into groundwater, have a definite minimum during the winter and two separate maxima during the spring and summer. The solid curves are smoother, as one would expect since they indicate the river flow into the lakes, thus incorporating some delay and smoothing due to water storage. During the spring, summer, and fall seasons, the modeled runoff greatly exceeds the observed river flow. Averaged over the entire year, the modeled inflow to Lake Superior is 1,954 m^3/s, and the observed inflow is 988 m^3/s. For Lake Michigan, the annual mean modeled inflow is 2,285 m^3/s, and the observed inflow is 1,252 m^3/s. Thus the model overestimates the total annual runoff by nearly a factor of 2. This perhaps represents a combined effect of the positive bias in precipitation and the

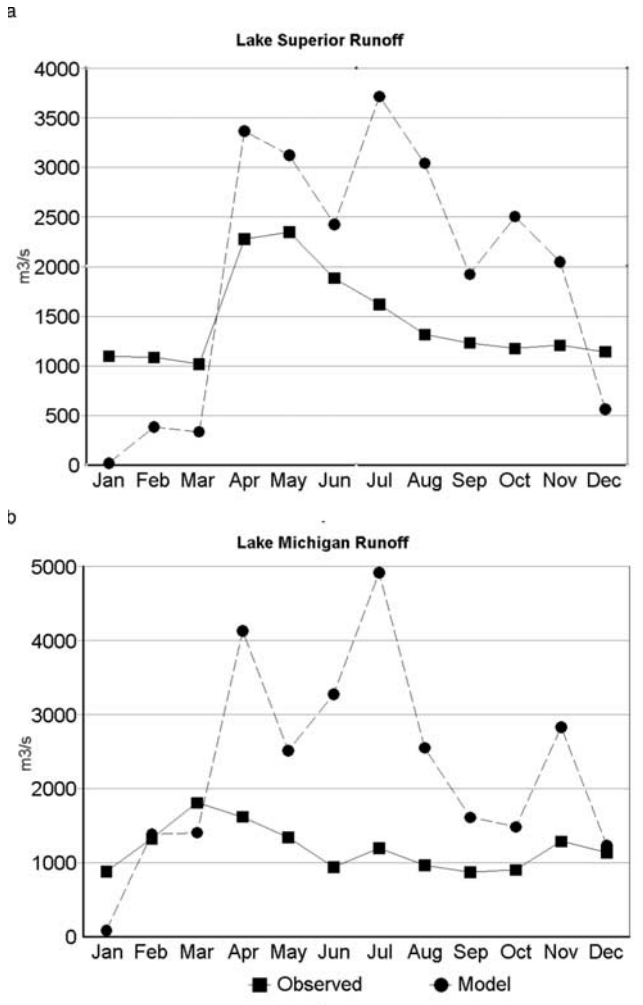

Figure 17. Runoff into (a) Lake Superior and (b) Lake Michigan during 1994 [from *Croley and Hunter*, 1994]. The solid curves use a weighted average of streamgage data based on the area of the subbasin which each gage represents. The dotted curves are the sum of the surface runoff and percolation of water downward out of the active soil layer; hence, they do not reflect the temporal lag and smoothing that result from water storage in inland surface reservoirs and groundwater.

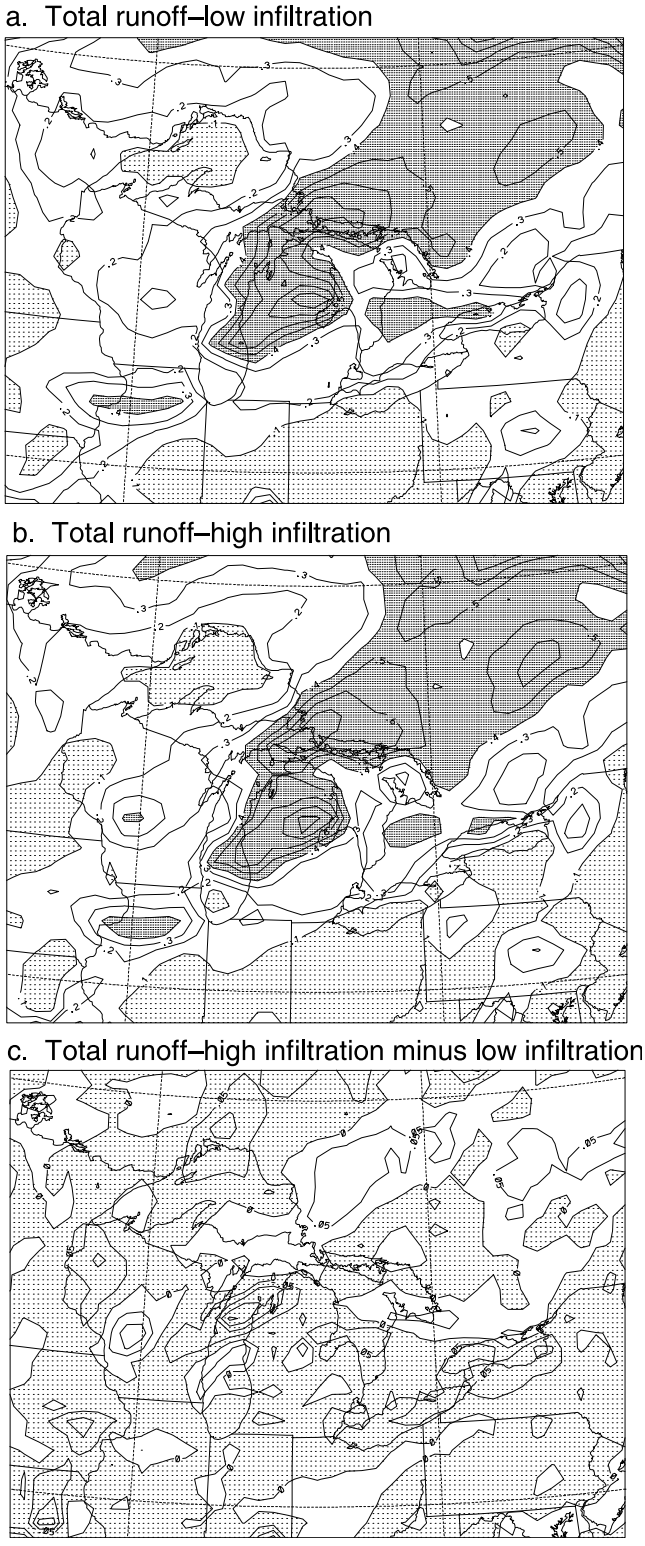

Figure 18. (a) The total runoff during July 1994 in the low infiltration case (sum of percolation and surface runoff); (b) in the high infiltration case; and (c) Figure 18b minus Figure 18a. In Figures 18a and 18b the contour interval is 0.1 mm/day; heavy shading indicates values greater than 0.4 mm/day, and light shading values less than 0.1 mm/day. In Figure 18c the contour interval is 0.05 mm/day, and light shading indicates values less than 0.

suppression of evapotranspiration by the presence of sustained stratus cloudiness.

[58] To compare the modified formulation of surface runoff, described in subsection 2.3.3, with the off-the-shelf formulation, a separate run was made with the older formulation. This has surface runoff calculated as the precipitation rate times the saturated fraction of the upper two soil layers (60 mm thickness of soil), forcing greater runoff than the formulation described in subsection 2.3.3, in which the saturated fraction is taken to the power of a soil type-dependent exponent, always quite large. The formulation in subsection 2.3.3, with the large exponent, will be called here the "high infiltration" case, while that with the exponent of unity will be called the "low infiltration" case.

[59] In the high infiltration case during July, the surface runoff is small, but much water is carried away from the soil through percolation through the bottom of the soil layers that are simulated (not shown). In the low infiltration case, the opposite occurs, with the greater loss going to surface runoff (not shown). The actual partitioning between surface runoff and deep soil percolation is not a well-observed quantity, so reliable validation is elusive. It is likely that the true partitioning lies somewhere between the extremes represented by these two formulations. It is heartening, though, that the total runoff (surface runoff plus deep soil percolation) is roughly the same in the two cases (Figure 18). While not a perfect match, especially in the dipole pattern over Wisconsin (Figure 18c), the general magnitudes and spatial patterns are well replicated. Total evaporation (not shown) shows similar agreement, and the fields of other atmospheric variables are nearly indistinguishable between the two cases. (The reader should be reminded that the total runoff and its components are defined quantities even over the lakes, because each grid box is assigned a percentage of land and of water, with surface flux calculations being carried out separately for them. Even where there is 100% water, land calculations are made, but all resultant fluxes are weighted at zero for their influence on the atmosphere, and likewise, they do not contribute to runoff into the lakes, such as that shown in Figure 17.)

6. Conclusions

[60] Some modifications to the framework of the Regional Atmospheric Modeling System (RAMS) have been incorporated into its implementation in the Coupled Hydrosphere-Atmosphere Research Model (CHARM). Chief among these are alterations aimed at adapting RAMS for use as a climate model.

[61] The resulting model is in reasonable agreement with observations in terms of air temperatures and precipitation. Another variable that is of particular interest for the intended hydrologic applications of CHARM is evapotranspiration. However, because of the lack of observations of this quantity in the Great Lakes basin, validation of this quantity is difficult. Simulated total annual runoff, which is derived from the balance of precipitation and evapotranspiration over land, is found to be nearly twice the observed amount. However, it is difficult to expect closer agreement, given the difficulty in predicting both precipitation and evapotranspiration and the amplifying effect on

the fractional error when considering a quantity that is the difference of two variables which are each subject to error. To use this runoff in further analysis, it is likely that empirical adjustment factors will need to be applied.

[62] One troubling model deficiency is that the mean sea level pressure and geopotential height at fixed pressure exhibit strong negative biases. This was found to be correlated to a general divergence of mass over the entire domain and a convergence of mass over the inner domain, leaving the outer margin, which sets the boundary conditions for pressure, strongly divergent and lowering its air pressure. Because the circulation depends on pressure gradients rather than the absolute value of pressure, the bias in pressure is not regarded as a very serious shortcoming for the simulation of scenarios. Also, in work to be presented separately, using data from a general circulation model as input for the lateral boundary conditions, this problem is strongly mitigated. A hypothesis for the cause of this is that a problem exists in translating the wind direction from the coordinates of the NCEP Reanalysis data to the CHARM grid.

[63] Another problem is excessive and persistent stratus cloudiness. This appears to be self-sustaining, as the presence of a cloud deck assures the divergence of longwave radiative flux at the cloud tops. This maintains a strong temperature inversion, which inhibits the exchange of moist boundary layer air with drier air from above. One future direction of inquiry that may aid in this respect would be to use a vegetation data set with greater horizontal resolution. As in *Weaver and Avissar* [2001] and *Avissar and Liu* [1996], land surface heterogeneity can force mesoscale circulations that will supplement the smaller-scale turbulence of the boundary layer, generally enhancing the vertical fluxes of moisture and sensible heat at heights at which the subgrid-scale (parameterized) turbulence is small. In the case of CHARM in the Great Lakes basin, these surface-forced mesoscale circulations may drive air to vertically mix across the temperature inversion. This effect is likely to feed back on itself by weakening the inversion. Support is given to this argument by Figure 14a, which gives evidence that the Great Lakes, which are one of the major sources of surface heterogeneity present in this domain, enhance the solar radiation at the surface by creating ''windows'' through the clouds.

[64] Another hypothesis for the formation of excessive clouds is the presence of evaporation from inland lakes (those other than the Great Lakes) with surface temperatures that are unrealistically assigned values that are based on spatial interpolation from ocean surface temperatures, often more than 1000 km distant.

[65] A version of the CHARM model and some of its results have been presented here. A primary purpose to which CHARM will be applied is the simulation of global warming effects on the hydrologic system of the Great Lakes basin. The effect of the pressure bias is unknown but is believed to be small, especially given that the pressure bias is greatly reduced when CHARM is driven with a general circulation model. The excessive cloudiness seems to contribute to warm biases during the winter, which inhibits ice formation on the lakes and snowpack on land. Additionally, CHARM can be applied to questions of the effects of land use change and, simulating shorter timescales, effects of teleconnection phenomena, such as the remote effects of El Niño–Southern Oscillation. Plans for further improvement to CHARM, in addition to those outlined above to mitigate pressure and cloud problems, include expanding its overall domain to encompass some of the Gulf of Mexico moisture source and more western regions of North America. We will also incorporate the superior land surface (particularly snow-related) parameterizations that have been incorporated in newer release versions of RAMS.

Appendix A: Calculation of Lowest Soil Layer's Effective Thermal Capacity

[66] Whereas the original RAMS formulation used a prescribed constant temperature for the lowest soil level, we allow it to vary, since we are interested in running CHARM over considerably longer timescales than have often been used with RAMS. The governing equation for diffusion of heat within the soil is

$$c\frac{\partial T}{\partial t} = \kappa\frac{\partial^2 T}{\partial z^2}, \tag{A1}$$

where c is the volumetric heat capacity of the soil and κ is its thermal diffusion coefficient. If the heat flux into an arbitrary boundary defining the top of a soil column has the form $Ae^{i\omega t}$, then we have the boundary conditions:

$$\frac{\partial T}{\partial z} = \frac{A}{\kappa}e^{i\omega t} \text{ at } z = 0 \tag{A2a}$$

$$\frac{\partial T}{\partial z} = 0 \text{ at } z = -\infty. \tag{A2b}$$

These equations apply regardless of the origin selected for the dimension z, so that the heat flux form in (A2a) can be prescribed at the surface or at any depth chosen as the origin. The soil temperature will take the form

$$T = \overline{T} + Be^{i(kz+\omega t-\phi)}, \tag{A3}$$

where $\overline{T}$ is the mean value of temperature in time and depth. Note that the sign convention here assures that perturbations in temperature will propagate downward if k and ω both have positive real parts. Substituting (A3) into (A1) under the constraint of (A2b) and solving for k, we get

$$k = \left(-i\frac{c\omega}{\kappa}\right)^{1/2} = \left(\frac{c\omega}{2\kappa}\right)^{1/2}(-i+1). \tag{A4}$$

Also, using (A2a) and (A3), and requiring that A and B are both real, $\phi = \pi/4$ and

$$B = A/\kappa|k| = A/(c\,\omega\kappa)^{1/2}. \tag{A5}$$

The above derivation gives a result equivalent to that found in *Bonan* [2002, p.189] (note that Bonan's use of c is heat capacity per unit mass, not volume, and the time origin is defined differently, eliminating ϕ).

[67] It is also possible to construct a theory that is equivalent in producing the same vertical heat flux at a given depth (for a single Fourier component in ω), under the assumption that the soil beneath that depth is a single heat reservoir. (We will use the top of our lowest soil layer as the depth below which to prescribe a single heat reservoir.) In this development, the temperature of the single heat reservoir will be denoted T_r, which will be a function of time but not of depth. With a heat flux of $Ae^{i\omega t}$ assigned at depth $z = 0$, as before:

$$c_a \frac{\partial T_r}{\partial t} = Ae^{i(\omega t - \phi_a)}, \tag{A6}$$

where c_a is an areal heat capacity, rather than the volumetric heat capacity of c above. From this,

$$T_r = -\frac{iA}{c_a \omega} e^{i(\omega t - \phi_a)}, \tag{A7}$$

where $\phi_a = \pi/2$. Unfortunately, this departs from equivalence in that this phase lag is different from that found for equations (A2)–(A5). In order to otherwise make the diffusion theory and the thermal reservoir theory equivalent relative to heat flux at $z = 0$, the real parts of the solutions in (A3) and (A7) must be equal. Thus $A = Bc_a\omega$ and, using (A4) and (A5),

$$c_a = \frac{\kappa Im(k)}{\omega} = \left(\frac{\kappa c}{2\omega}\right)^{1/2}. \tag{A8}$$

[68] Values of c_a and k are stated as functions of ω, so it is necessary to choose a relevant Fourier component on which to base this formulation. The two dominant modes of forcing that we expect will have periods of 1 day and 1 year. Typical values of κ and c (for loam at 50% saturation) are.17 J m^{-1} s^{-1} K^{-1} and 1.9×10^6 J m^{-3} K^{-1}, respectively. From (A4), then, for a period of 1 year, the e-folding depth ($1/k$) is 0.95 m and from (A8), c_a is 9.0×10^5 J m^{-2} K^{-1}. For a period of 1 day, the e-folding depth is 0.05 m and c_a is 4.7×10^4 J m^{-2} K^{-1} [see also *Bonan*, 2002, p. 189]. Thus the temperature response to heat input that cycles at a period of 1 day will decay very strongly before reaching a depth of 0.5 m, the top of our lowest soil layer, allowing the thermal response to the daily heating cycle to be explicitly represented by the soil model. Forcings with periods of several days will also be strongly damped before reaching the bottom layer of the soil model. Because of this, it is safe to calculate c_a based on the annual cycle. Interannual variations in soil temperature will be overestimated and variations on harmonics of the annual cycle will be underestimated, but only by a small amount, and the annual mode will dominate.

[69] Therefore the deepest soil layer has been formulated as a heat reservoir of constant areal heat capacity as given by (A8), with c and κ assumed to maintain constant values appropriate for the prescribed soil type at 50% saturation. Were this 50% saturation assumption and the assumption of a pure annual sinusoidal signal true (which they are not in practice), and also ignoring the difference in phase lag between the heat flux and the temperature response between the two formulations, the heat fluxes that the overlying layers would "see" would be equivalent to those that would result from simulating an infinite soil depth.

Appendix B: Linearized Definition of Equation of Vertical Motion and "Hydrostatic" Under Exner Framework

[70] One feature of RAMS that plays a role in the low mean sea level pressures and tropospheric geopotential heights is the use of a linearized version of the equations of vertical motion, based on a reference profile of temperature and Exner function, a proxy for pressure. The Exner function, Π, is defined as $\Pi = c_p(p/p_0)^{2/7}$, where c_p is the heat capacity of dry air at constant pressure, 1004 J kg^{-1} K^{-1}; p is pressure; and p_0 is reference pressure of 1000 hPa. Using the Cartesian z as the vertical coordinate, the vertical component of the equation of motion is

$$\frac{\partial w}{\partial t} = -g - \theta_e \frac{\partial \Pi}{\partial z}, \tag{B1}$$

where w is vertical velocity, g is acceleration due to gravity, and θ_e is equivalent potential temperature. Expanding θ_e as $\theta_0 + \theta'$ and Π as $\Pi_0 + \Pi'$, the full equation is

$$\frac{\partial w}{\partial t} = -g - \theta_0 \frac{\partial \Pi_0}{\partial z} - \theta' \frac{\partial \Pi_0}{\partial z} - \theta_0 \frac{\partial \Pi'}{\partial z} - \theta' \frac{\partial \Pi'}{\partial z}. \tag{B2}$$

The reference state is defined so that $\partial\Pi_0/\partial z = -g/\theta_0$, leaving

$$\frac{\partial w}{\partial t} = -\theta' \frac{\partial \Pi_0}{\partial z} - \theta_0 \frac{\partial \Pi'}{\partial z} - \theta' \frac{\partial \Pi'}{\partial z}. \tag{B3}$$

[71] In practice, however, RAMS uses only the linear terms, eliminating the last term in (B3). This is not well justified, however, as θ' can take on values that are a significant fraction of θ_0. In RAMS, the reference state (a single vertical profile of Π_0 and θ_0) is chosen by extracting the initial profile of equivalent potential temperature from the grid point with the lowest surface elevation. In the present model domain, this is located near the southeast corner of the full domain, at the first grid space on the Atlantic Ocean as one traverses the southernmost grid row from west to east. Air temperatures there are considerably higher than in many other areas at the time of model initialization on January 1, 1993. The first few time steps of the model run were scrutinized, and some typical values of the variables were extracted for a terrestrial grid point far away from the reference point: $\theta' = -30$ K; $\partial\Pi'/\partial z = 0.0039$ m s^{-2} K^{-1}; $\theta_0 = 290$ K; $\partial\Pi_0/\partial z = 0.0338$ m s^{-2} K^{-1}. Thus the first term on the right-hand side of (B3) is 1.014 m s^{-2}, the second term is -1.131 m s^{-2}, and the third term is 0.117 m s^{-2}. In the full form of (B3), these balance, yielding no vertical acceleration, or a hydrostatic condition, but by eliminating the final term, they are out of balance, yielding vertical acceleration. This vertical motion works toward the restoration of approximate hydrostatic balance, with this balance redefined as a balance between only the first two terms on the right side of (B3). Using the

full form of (B3), hydrostatic balance (the condition of no vertical acceleration) is defined by

$$\frac{\partial \Pi'}{\partial z} = -\frac{g\theta'}{\theta_0(\theta_0 + \theta')}. \tag{B4}$$

Using the linearized form of (B3), a change results:

$$\frac{\partial \Pi'}{\partial z} = -\frac{g\theta'}{\theta_0^2}. \tag{B5}$$

[72] As approximated by a first-order Taylor expansion, the hydrostatic gradient of Exner function with height given in (B4) is always greater than that given in (B5) by $g\theta'^2/\theta_0^3$, which in turn is on the order of $(\theta'/\theta_0)^2$ times $\partial\Pi_0/\partial z$. Thus, if θ' is approximately 10% of the magnitude of θ_0, $\partial\Pi/\partial z$ can be off by 1%. If this is true through the entire atmospheric column, surface pressure may be off by 1% or roughly 10 hPa. As of RAMS release version 4.4, the linearized version of (B3) is still used, rather than the full version.

[73] **Acknowledgments.** This is GLERL contribution 1316. Thanks to T. Croley and J. McQueen for their assistance in initiating this modeling effort. Thanks to J. Lenters and anonymous reviewers for their comments on various drafts of this paper.

References

André, J. C., G. De Moor, P. Lacarrère, G. Therry, and R. du Vachat (1978), Modeling the 24-hour evolution of the mean and turbulent structures of the planetary boundary layer, *J. Atmos. Sci.*, *35*, 1861–1883.

Avissar, R., and Y. Liu (1996), Three-dimensional numerical study of shallow convective clouds and precipitation induced by land-surface forcing, *J. Geophys. Res.*, *101*, 7499–7518.

Avissar, R., and Y. Mahrer (1988), Mapping frost-sensitive areas with a three-dimensional local-scale numerical model. part I: Physical and numerical aspects, *J. Appl. Meteorol.*, *13*, 289–297.

Bates, G. T., F. Giorgi, and S. W. Hostetler (1993), Toward the simulation of the effects of the Great Lakes on regional climate, *Mon. Weather Rev.*, *121*, 1373–1387.

Bates, G. T., S. W. Hostetler, and F. Giorgi (1995), Two-year simulation of the Great Lakes region with a coupled modeling system, *Mon. Weather Rev.*, *123*, 1505–1522.

Boer, G. J., G. M. Flato, and D. Ramsden (2000), A transient climate change simulation with greenhouse gas and sulphate aerosol forcing: Projected climate to the twenty-first century, *Clim. Dyn.*, *16*, 427–450.

Bonan, G. B. (2002), *Ecological Climatology: Concepts and Applications*, 678 pp., Cambridge Univ. Press, New York.

Businger, J. A. (1966), Transfer of momentum and heat in the planetary boundary layer, in *Proceedings of a Symposium on Arctic Heat Budget and Atmospheric Circulation*, pp. 305–331, The RAND Corp., Santa, Monica, Calif.

Charnock, H. (1955), Wind stress over a water surface, *Q. J. R. Meteorol. Soc.*, *81*, 639–640.

Chen, C., and W. R. Cotton (1983), A one-dimensional simulation of the stratocumulus-capped mixed layer, *Boundary Layer Meteorol.*, *25*, 289–321.

Chen, C., and W. R. Cotton (1987), The physics of the marine stratocumulus-capped mixed layer, *J. Atmos. Sci.*, *44*, 2951–2977.

Clapp, R., and G. Hornberger (1978), Empirical equations for some soil hydraulic properties, *Water Resour. Res.*, *14*, 601–604.

Coordinating Committee on Great Lakes Basic Hydraulic and Hydrologic Data (1977), Coordinated Great Lakes physical data, 12 pp., U.S. Army Corps of Eng., Detroit.

Cotton, W. R., M. A. Stephens, T. Nehrkorn, and G. J. Tripoli (1982), The Colorado State University three-dimensional cloud/mesoscale model-1982. part II: An ice phase parameterization, *J. Rech. Atmos.*, *16*, 295–320.

Croley, T. E., II (1983), Great Lakes Basins (U.S.A.-Canada) runoff modeling, *J. Hydrol.*, *64*, 135–158.

Croley, T. E., II (1989), Verifiable evaporation modeling on the Laurentian Great Lakes, *Water Resour. Res.*, *25*, 781–792.

Croley, T. E., II (1990), Laurentian Great Lakes double-CO_2 climate change hydrological impacts, *Clim. Change*, *17*, 27–47.

Croley, T. E., II (1992), Long-term heat storage in the Great Lakes, *Water Resour. Res.*, *28*, 69–81.

Croley, T. E., II (2003), Great Lakes climate change hydrologic impact assessment: IJC Lake Ontario-St. Lawrence River regulation study, *GLERL Tech. Memo. TM-126*, 77 pp., Great Lakes Environ. Res. Lab., Ann Arbor, Mich.

Croley, T. E., II, and R. A. Assel (1994), A one-dimensional ice thermodynamics model for the Laurentian Great Lakes, *Water Resour. Res.*, *30*, 625–639.

Croley, T. E., II, and H. C. Hartmann (1989), Effects of climate changes on the Laurentian Great Lakes levels, in *The Potential Effects of Global Climate Change on the United States*, *Appendix A: Water Resources*, edited by J. B. Smith and D. A. Tirpak, *Rep. EPA-230-05-89-051*, pp. 4-1–4-34, U. S. Environ. Prot. Agency, Washington, D. C.

Croley, T. E., II, and T. S. Hunter (1994), Great Lakes monthly hydrologic data, *GLERL Tech. Memo. TM-83*, 12 pp., Great Lakes Environ. Res. Lab., Ann Arbor, Mich. (Available at ftp://ftp.glerl.noaa.gov/publications/tech_reports/glerl-083/UpdatedFiles)

Croley, T. E., II, P. Y. T. Louie, and L. Mortsch (1991), CCC GCM 2xCO_2 hydrological impacts on the Great Lakes, Final Report Appendix Section, Subtask 19.1.2, Climate Scenario Development, Task 19.1, Climate and Climate Change, Task Group 2, Working Committee 3, Phase II of the International Joint Commission Water Levels Reference Study, 25 pp., Int. Joint Comm., Washington, D. C.

Dickinson, R. E., R. M. Errico, F. Giorgi, and G. T. Bates (1989), A regional climate model for the western United States, *Clim. Change*, *15*, 383–422.

Giorgi, F., and G. T. Bates (1989), The climatological skill of a regional model over complex terrain, *Mon. Weather Rev.*, *117*, 2325–2347.

Gordon, C., C. Cooper, C. A. Senior, H. Banks, J. M. Gregory, T. C. Johns, J. F. B. Mitchell, and R. A. Wood (2000), The simulation of SST, sea ice extents and ocean heat transports in a version of the Hadley Centre coupled model without flux adjustments, *Clim. Dyn.*, *16*, 147–168.

Goyette, S., N. A. McFarlane, and G. M. Flato (2000), Application of the Canadian Regional Climate Model to the Laurentian Great Lakes region: Implementation of a lake model, *Atmos. Ocean*, *38*, 481–503.

Hansen, J., I. Fung, A. Lacis, D. Rind, S. Lebedeff, R. Ruedy, G. Russell, and P. Stone (1988), Global climate changes as forecast by the Goddard Institute for Space Studies three-dimensional model, *J. Geophys. Res.*, *93*, 9341–9364.

Hartmann, H. C. (1990), Climate change impacts on Laurentian Great Lakes levels, *Clim. Change*, *17*, 49–67.

Hjelmfelt, M. R. (1990), Numerical study of the influence of environmental conditions on lake-effect snowstorms over Lake Michigan, *Mon. Weather Rev.*, *118*, 138–150.

Hjelmfelt, M. R., and R. R. Braham Jr. (1983), Numerical simulation of the airflow over Lake Michigan for a major lake-effect snow event, *Mon. Weather Rev.*, *111*, 205–219.

Hostetler, S. W., G. T. Bates, and F. Giorgi (1993), Interactive coupling of a lake thermal model with a regional climate model, *J. Geophys. Res.*, *98*, 5045–5057.

Intergovernmental Panel on Climate Change (1990), *Climate Change: The IPCC Scientific Assessment*, edited by J. T. Houghton, G. J. Jenkins, and J. J. Ephraums, 365 pp., Cambridge Univ. Press, New York.

Intergovernmental Panel on Climate Change (1996), *Climate Change 1995: The Science of Climate Change*, edited by J. T. Houghton et al., 572 pp., Cambridge Univ. Press, New York.

Intergovernmental Panel on Climate Change (2001), *Climate Change 2001: The Scientific Basis*, edited by J. T. Houghton et al., 944 pp., Cambridge Univ. Press, New York.

Kalnay, E., et al. (1996), The NCEP/NCAR 40-year Reanalysis Project, *Bull. Am. Meteorol. Soc.*, *77*, 437–471.

Klemp, J. B., and R. B. Wilhelmson (1978a), The simulation of three-dimensional convective storm dynamics, *J. Atmos. Sci.*, *35*, 1070–1096.

Klemp, J. B., and R. B. Wilhelmson (1978b), Simulations of right- and left-moving storms produced through storm splitting, *J. Atmos. Sci.*, *35*, 1097–1110.

Liston, G. E., and R. A. Pielke (2001), A climate version of the Regional Atmospheric Modeling System, *Theor. Appl. Climatol.*, *68*, 155–173.

Lofgren, B. M., F. H. Quinn, A. H. Clites, R. A. Assel, A. J. Eberhardt, and C. L. Luukkonen (2002), Evaluation of potential impacts on Great Lakes water resources based on two GCM climate scenarios, *J. Great Lakes Res.*, *28*, 537–554.

Louis, J.-F. (1979), A parametric model of vertical eddy fluxes in the atmosphere, *Boundary Layer Meteorol.*, *17*, 187–202.

Lyons, W. A., and H. S. Cole (1976), Photochemical oxidant transport: Mesoscale lake breeze and synoptic-scale aspects, *J. Appl. Meteorol.*, *15*, 733–743.

Mahrer, Y., and R. A. Pielke (1977), A numerical study of the airflow over irregular terrain, *Contrib. Atmos. Phys.*, *50*, 98–113.
Manabe, S., and R. J. Stouffer (1994), Multiple-century response of a coupled ocean-atmosphere model to an increase of atmospheric carbon dioxide, *J. Clim.*, *7*, 5–23.
Matthews, E. (1983), Global vegetation and land use: New high-resolution data bases for climate studies, *J. Clim. Appl. Meteorol.*, *22*, 474–487.
McCumber, M. C., and R. A. Pielke (1981), Simulation of the effects of surface fluxes of heat and moisture in a mesoscale numerical model. part I: Soil layer, *J. Geophys. Res.*, *86*, 9929–9938.
Mellor, G. L., and T. Yamada (1974), A hierarchy of turbulence closure models for planetary boundary layers, *J. Atmos. Sci.*, *31*, 1791–1806.
Pielke, R. A., et al. (1992), A comprehensive meteorological modeling system-RAMS, *Meteorol. Atmos. Phys.*, *49*, 69–91.
Pinker, R. T., and I. Laszlo (1992), Modeling surface solar irradiance for satellite applications on a global scale, *J. Appl. Meteorol.*, *31*, 194–211.
Reynolds, R. W. (1988), A real-time global sea surface temperature analysis, *J. Clim.*, *1*, 75–86.
Sousounis, P. J., and J. M. Fritsch (1994), Lake-aggregate mesoscale disturbances. part II: A case study of the effects on regional and synoptic-scale weather systems, *Bull. Am. Meteorol. Soc.*, *75*, 1793–1811.
Sousounis, P. J., and H. N. Shirer (1992), Lake-aggregate mesoscale disturbances. part I: Linear analysis, *J. Atmos. Sci.*, *49*, 80–96.
Stouffer, R. J., and S. Manabe (1999), Response of a coupled ocean-atmosphere model to increasing atmospheric carbon dioxide: Sensitivity to the rate of increase, *J. Clim.*, *12*, 2224–2237.
Tremback, C. J. (1990), Numerical simulation of a mesoscale convective complex: Model development and numerical results, Ph.D. dissertation, 247 pp., Dep. of Atmos. Sci., Colo. State Univ., Fort Collins.
Tremback, C. J., G. J. Tripoli, and W. R. Cotton (1985), A regional scale atmospheric numerical model including explicit moist physics and a hydrostatic time-split scheme, paper presented at 7th Conference on Numerical Weather Prediction, Am. Meteorol. Soc., Montréal, Québec, Canada, 17–20 June.
Tripoli, G. J., and W. R. Cotton (1980), A numerical investigation of several factors contributing to the observed variable intensity of deep convection over south Florida, *J. Appl. Meteorol.*, *19*, 1037–1063.
Tripoli, G. J., and W. R. Cotton (1982), The Colorado State University three-dimensional cloud/mesoscale model—1982. part I: General theoretical framework and sensitivity experiments, *J. Rech. Atmos.*, *16*, 185–219.
Weaver, C. P., and R. Avissar (2001), Atmospheric disturbances caused by human modification of the landscape, *Bull. Am. Meteorol. Soc.*, *82*, 269–281.
Yamada, T., and G. Mellor (1975), A simulation of the Wangara atmospheric boundary layer data, *J. Atmos. Sci.*, *32*, 2309–2329.

B. M. Lofgren, Great Lakes Environmental Research Laboratory, NOAA, 2205 Commonwealth Blvd., Ann Arbor, MI 48105-2945, USA. (brent.lofgren@noaa.gov)